

SLOVENSKÝ ČASOPIS PRE GEOMETRIU A GRAFIKU ročník 22, číslo 43, 2025 ISSN 1336-524X **G** Slovenský časopis pre geometriu a grafiku

Ročník 22 (2025), číslo 43 ISSN 1336-524X

Vydáva:

Slovenská spoločnosť pre Geometriu a Grafiku

SSGG

Vedúca redaktorka:

Daniela Velichová

Výkonné redaktorky:

Dagmar Szarková Daniela Richtáriková

Redakčná rada:

Ján Čižmár Andrej Ferko Pavel Chalmovianský Mária Kmeťová Margita Vajsáblová G je vedecký časopis pre geometriu a grafiku publikujúci originálne vedecké práce, prehľady a informatívne články, krátke referáty, odborné príspevky, analýzy, aktuality a rešerše z rôznych odvetví geometrie (elementárna, deskriptívna, konštrukčná, projektívna, analytická, diferenciálna, algebrická, počítačová, výpočtová, konečná, neeuklidovská) a topológie, geometrického modelovania a počítačovej grafiky, v oblasti základného teoretického výskumu, v oblasti výučby geometrie na všetkých typoch a metodológie škôl, z histórie vývoja a z aplikácií geometrie a geometrických metód v rôznych vedeckých, spoločenských a technických disciplínach.

Redakcia: Slovenská spoločnosť pre Geometriu a Grafiku

IČO: 31 816 304

Ústav matematiky a fyziky, Strojnícka fakulta Slovenská technická univerzita v Bratislave

Námestie slobody 17 812 31 Bratislava

Objednávky, reklamácie a predplatné vybavuje:

Redakcia G - SSGG

ÚMF SjF STU, Námestie slobody 17, 812 31 Bratislava

ssgg@ssgg.sk

Periodicita: Časopis vychádza dvakrát do roka v náklade 200 kusov.

Ročné predplatné bez poštovného a balného je 20,- Eur.

Evidenčné číslo EV 3228/09

Informácie a pokyny pre autorov na adrese: www.ssgg.sk

Tlačí: ForPress Nitrianske tlačiarne, s.r.o.

Časopis G je evidovaný v: Zentralblatt für Mathematik

Copyright © SSGG september 2025, Bratislava, číslo 1/2025

Všetky práva vyhradené. Žiadna časť tejto publikácie sa nesmie reprodukovať, ukladať do informačných systémov alebo rozširovať akýmkoľvek spôsobom, či už elektronicky, mechanicky, fotografickou reprodukciou alebo ináč, bez predchádzajúceho písomného súhlasu vlastníkov práv. Všetky príspevky uverejnené v časopise prešli odbornou recenziou.

SLOVENSKÝ ČASOPIS PRE GEOMETRIU A GRAFIKU SLOVAK JOURNAL FOR GEOMETRY AND GRAPHICS

ročník 22, číslo 43, 2025 volume 22, number 43, 2025



Obsah – Contents

| The curves of Eduard Lehr Krivky Eduarda Lehra | 5 |
|---|----|
| Péter Salvi | |
| MST-based clustering for curve and surface reconstruction Klastrovanie na báze MST pre rekonštrukciu kriviek a plôch Šárka Voráčová | 25 |
| Pedal curves – a playground for generalizations Úpätnice – ihrisko pre zovšeobecňovanie Gunter Weiss | 33 |

SLOVENSKÁ SPOLOČNOSŤ



PRE GEOMETRIU A GRAFIKU

Nezisková vedecká spoločnosť pre rozvoj geometrie a počítačovej grafiky

zaregistrovaná dňa 13.5.2002 na Ministerstve vnútra SR ponúka všetkým záujemcom individuálne alebo kolektívne členstvo. Elektronickú prihlášku nájdete na domovskej stránke spoločnosti.

Cieľom spoločnosti je stimulovať vedecký výskum, aplikácie i pedagogickú prácu a metodiku vyučovania v oblasti geometrie a počítačovej grafiky.

Spoločnosť pôsobí na celom území Slovenskej republiky a jej poslaním je:

- a) podporovať rozvoj geometrie a počítačovej grafiky a ich vzájomnej interakcie
- b) presadzovať kvalitu geometrického a grafického vzdelania na všetkých typoch škôl v SR
- c) spolupracovať s medzinárodnými spoločnosťami a organizáciami rovnakého zamerania
- d) podieľať sa na organizácii vedeckých podujatí, konferencií, seminárov a sympózií o geometrii a počítačovej grafike
- e) publikovať vedecký časopis s názvom G venovaný geometrii a grafike
- f) rozvíjať vlastnú edičnú a publikačnú činnosť
- g) získať priazeň a členstvo organizácií aj jednotlivcov.

Vítané sú všetky ďalšie aktivity – diskusné fórum na Internete, softvérový bazár, workshopy, e-learningové kurzy ai., ktoré možno vykonávať pod hlavičkou spoločnosti.

Spoločnosť SSGG Ústav matematiky a fyziky Strojnícka fakulta STU v Bratislave Námestie slobody 17, 812 31 Bratislava, SR e-mail: ssgg@ssgg.sk, URL: www.ssgg.sk

The curves of Eduard Lehr

Péter Salvi

Abstrakt

Trieda kriviek, ktorých krivosť je funkciou dĺžky oblúka, goniometrickou sa počas minulého storočia mnohokrát objavovala v rôznych kontextoch. prvý sa jej štúdiu venoval Eduard Lehr v relatívne neznámej práci. Vzhľadom na obnovený záujem o túto problematiku v oblasti estetických kriviek [8], zhrnieme v tomto článku jej najdôležitejšie výsledky.

Kľúčové slová: estetické krivky, trig-estetické krivky, elastika

Abstract

The class of curves whose curvature is a trigonometric function of the arc length has appeared multiple times in the last century, in different contexts. It was first studied by Eduard Lehr, in a relatively obscure work. Due to renewed interest in it within the field of aesthetic curves [8], we summarize its most important results in this paper.

Keywords: aesthetic curves, trig-aesthetic curves, elastica

1 Introduction

Aesthetic plane curves are often defined by their Cesàro equation, i.e., the curvature as a function of arc length. A well-known example is the class of *log-aesthetic* curves [5], but a few other types are also briefly explored in Alfred Gray's textbook (Sections 5.3–5.4) [1], including one where

$$\kappa(s) = c\sin s,\tag{1}$$

with c being an arbitrary constant. This is quoted in Stephen Wolfram's A New Kind of Science (p. 418, example (j) in the figure) [9], and the corresponding note on p. 1009 adds that the case of $\kappa(s) = a \sin(bs)$ 'was studied by Eduard Lehr in 1932'. Lehr's dissertation [3] was already in Gray's bibliography, although no explicit reference was made there.

The curve in question, in slightly different form, has been used in geophysics to model river meandering since the 1960s [4], as it closely resembles the naturally occurring shape of *elastica*. There it is called a *sine-generated* curve, and it is defined by its tangent angle:

$$\theta(s) = \omega \sin \frac{2\pi s}{L}.\tag{2}$$

Here ω is the maximum turning angle and L is the total length. Deriving this we arrive at the Cesàro equation

$$\kappa(s) = \frac{2\pi\omega}{L}\cos\frac{2\pi s}{L}.\tag{3}$$

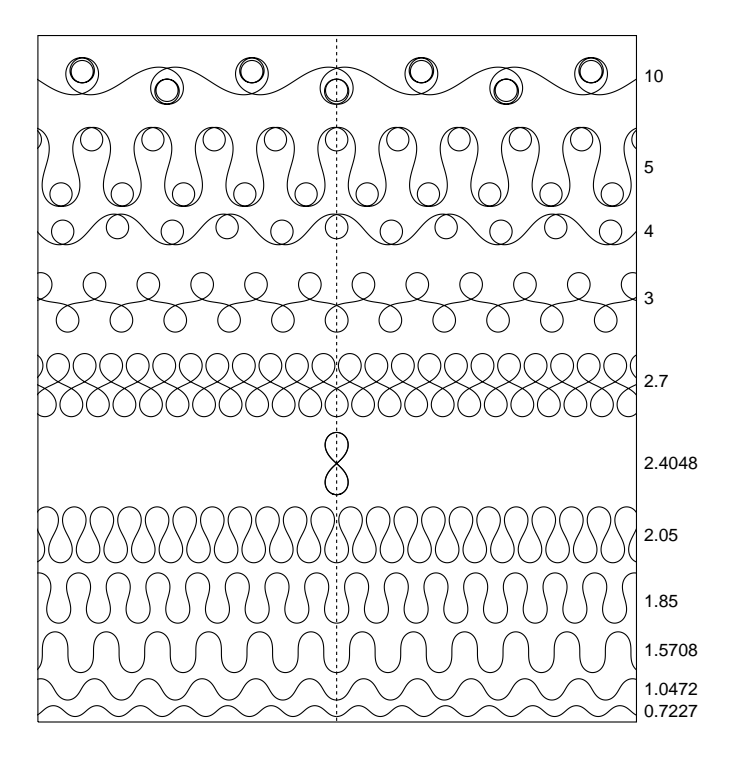


Fig. 1. Trig-aesthetic curves (Eq. 4) for various c values. The s=0 points are always placed on the dotted line.

Recently, the simplified formulation

$$\kappa(s) = \cos\frac{s}{c} \tag{4}$$

was proposed as an intrinsically fair curve representation, by the name *trig-aesthetic* curve (see Fig. 1) [8].

It appears that the first study of this class of curves was carried out by Lehr, but his work is in German, and it is available only in a handful of libraries. This paper aims to summarize his most important results.

2 Who was Eduard Lehr?

Eduard Lehr was born in 25 July 1906, in Ingolstadt, to Franz Xavier Lehr, a senior teacher and headmaster in Munich. He studied to be a teacher and passed the examinations in 1929–30, while also working as an assistant for descriptive geometry at the Technical University of Munich (then still called *Technische Hochschule München*). He wrote his dissertation there in 1932, first under the "father of glacier photogrammetry", Sebastian Finsterwalder, then—after his advisor's retirement—under Josef Lense (known from the Lense–Thirring effect) [7].

He started his military training in 1936, and did military service during the Second World War with various anti-aircraft artillery batallions in Nuremberg, Darmstadt and other places, eventually rising to the rank of first lieutenant of the reserve. According to the assessments in his military records (see Fig. 2a), he was a slender man of small build, quiet and earnest, somewhat shy, but possessed a strong will. He lacked leadership skills, however, and in 1941, upon being





(a) Excerpt from the military records

(b) From his obituary

Fig. 2. Photos of Eduard Lehr.

appointed commander of a coastal battery, he suffered a nervous breakdown and requested a transfer to the weather service.

In 1942 he married Barbara Horras, the daughter of a locomotive driver, but she died pregnant in an air raid in 1945, leaving Lehr a childless widower. After the war, he was briefly suspended from teaching due to his membership in the Nazi Party and other pro-nazi organizations. Classified as a minor offender, he was reinstated in 1947; he taught mathematics and physics in Traunstein and later in Munich. His last workplace was the Max-Planck-Gymnasium, where he also acted as director from 1952 until his untimely death in 1955 (see Fig. 2b).

Apart from his dissertation, only one other scientific work is attributed to him, although we have not been able to locate it: "Über die Dreiecksteilung von Vieleckern durch Ecktransversalen" (On the triangulation of polygons using vertex transversals).

3 Lehr's curves

The dissertation of Eduard Lehr bears the title 'On curves whose curvature is a periodic function of arc length' (Fig. 3). It is dedicated to the analysis of the curve family defined by the intrinsic equation

$$\kappa = \frac{1}{\rho} = a + b\cos(cs). \tag{5}$$

Note the presence of the additional term a, which—as we will see below—adds many different shapes to those in Equations (1) or (4).

In the following, we will distinguish the shape parameter of trig-aesthetic curves (Eq. 4) with a hat (\hat{c}) to differentiate it from the c parameter in Eq. (5).

In the rest of this section, we will go through the main results of Lehr's work, following largely its original structure.

Über die Kurven, deren Krümmung eine periodische Funktion des Bogens ist. Technischen Hochschule München zur Erlangung der Würde eines Doktors der technischen Wissenschaften genehmigte Abhandlung. Vorgelegt von Studienassessor Eduard Lehr, geboren zu Ingolstadt. Berichterstatter; o. Prof. Geh. Rat Dr. rer. nat. Dr. Dr. d. techn. Wissensch. eh. Dr. phil. eh. Sebastian Finsterwalder. 2. Berichterstatter: o. Prof. Dr. phil. Joseph Lense. Tag der Einreichung der Arbeit: 21. I. 1932. Tag der Annahme der Arbeit: 24. II. 1932.

Fig. 3. The cover page of Eduard Lehr's dissertation.

3.1 General properties

We can assume without loss of generality that $a \ge 0$, b > 0 and c > 0 (the b = 0 and c = 0 cases are just circles). Due to the symmetric shape of the cosine function, it is enough to examine a half period of the curve, starting from $s_0 = 0$ and ending in $s_1 = \frac{\pi}{c}$. All symbols with indices 0 and 1 relate to these endpoints, e.g. θ_0 is the starting tangent angle. The points themselves are denoted by P_0 and P_1 . Symbols with a bar (e.g. \bar{s}) are associated with the inflection point. (Notations are as in Lehr's work, except for θ and ϕ , which have their roles reversed. Additionally, curvature (κ) is often used, while only the radius of curvature (ρ) is seen in the original.)

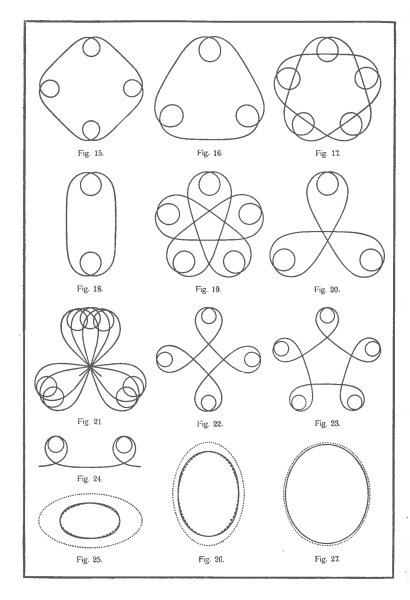
Since $\rho \neq 0$ there are no cusps, and the curvature extrema are in the endpoints. We only have an inflection when $a \leq b$ (which is actually just a flat point when a = b). The endpoints are the only vertices (i.e., points where $d\kappa/ds = 0$).

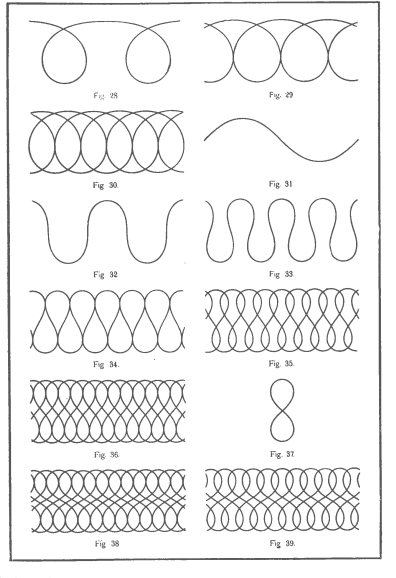
The shape is defined by the ratio a:b:c, so we have only 2 degrees of freedom if we do not care about the scaling. A simple convention is to fix $\kappa_0=a+b=1$. To exclude rotations we will also assume $\theta_0=0$, so

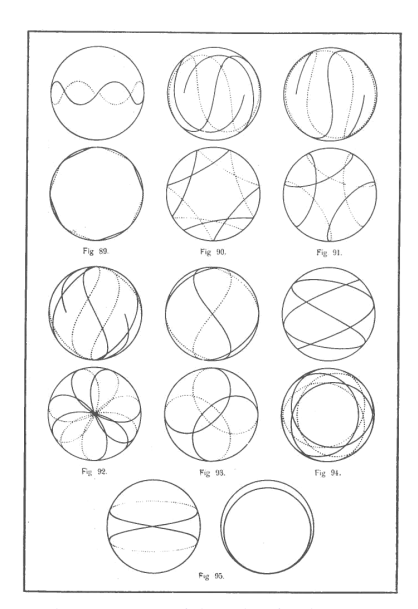
$$\theta = as + \frac{b}{d}\sin(cs)$$
 \Rightarrow $\theta_1 = \frac{a\pi}{c}$. (6)

Consequently, when $\frac{a}{c}$ is an integer, the tangents at the endpoints are parallel. If in addition P_1 is on the normal line of P_0 the curve is closed. When $\frac{a}{c}$ is not an integer, the whole periodic curve remains inside a circle around M, where M is the intersection of the normals at the endpoints. It becomes a closed curve only when

$$\theta_1 = m\pi + \frac{\nu}{n}\pi,\tag{7}$$







(a) Two pages with planar curves

(b) A page with spherical curves

Fig. 4. Curves drawn by Eduard Lehr.

where m, n and ν are integers, ν and n are relative prime, and $\nu < n$. In this case, the curve will make n periods and ν full turns until it closes in itself, making m extra loops at the vertices. (See also Section 3.5 and Appendix A.)

We also define the excess angle as

$$\phi = \bar{\theta} - \theta_1 = \frac{1}{c} \left(\sqrt{b^2 - a^2} - a \arccos \frac{a}{b} \right). \tag{8}$$

Note that ϕ is imaginary for a>b. Lehr regards the $\phi=0$ (i.e., a=b), $\theta_1>0$ case as the *base form*; other notable forms are (i) the *intermediary forms*, when $\theta_1>0$ and $0<|\phi|<\infty$ (i.e., $0\neq a\neq b\neq 0$), and (ii) that which are now called *trig-aesthetic* curves (cf. Eq. 4), when a=0. All other cases are either circles or straight lines.

3.2 Related curves

Here we examine some derived curve expressions.

3.2.1 Evolute

Following Cesàro [2] (Section II, Eq. 13), Lehr defines a series of radii of curvature as

$$\rho_{(0)} = \rho, \qquad \qquad \rho_{(k)} = \rho \frac{\mathrm{d}}{\mathrm{d}s} \rho_{(k-1)}.$$
(9)

(Here we also deviate slightly from Lehr's notation, who uses $\rho', \rho'', \rho''', \ldots$ for the series of radii of curvature.)

Then the arc length of the evolute is $s' = \rho$, its radius of curvature is $\rho' = \rho_{(1)}$; the tangent angle is the same as of the original curve, i.e., $\theta' = \theta$. Consequently, the evolute has cusps at the endpoints.

The differential equation form of our curves is

$$\rho_{(1)}^2 = c^2 \rho^4 (b^2 \rho^2 - (1 - a\rho)^2), \tag{10}$$

from which the intrinsic equation of the evolute is

$$\rho'^2 = c^2 s'^4 (b^2 s'^2 - (1 - as')^2). \tag{11}$$

3.2.2 Offset

The curve at distance p has arc length $S=s+p\theta$, radius of curvature $R=\rho+p$, and tangent angle $\Theta=\theta$. Since $\rho=-p$ implies a zero radius of curvature, there will be a cusp there, except when it coincides with the endpoint.

We can express our curve based on its offset:

$$S = \frac{p}{c} \sqrt{b^2 - \left(\frac{1}{R - p} - a\right)^2} + \frac{1 + ap}{c} \arccos \frac{\frac{1}{R - p} - a}{b},\tag{12}$$

which becomes purely algebraic in the case of $p = -\frac{1}{a}$:

$$(aR+1)^2(a^2c^2S^2-b^2)+a^4R^2=0. (13)$$

The intrinsic equation of the offset (from Eq. 10) is

$$P^{2} = c^{2}(R - p)^{4}(b^{2}(R - p)^{2} - (1 + ap - aR)^{2}).$$
(14)

The meaning of P is not discussed, but it is evidently

$$P = \rho_{(1)} = R \cdot \frac{\mathrm{d}R}{\mathrm{d}S}.\tag{15}$$

3.2.3 Involute

The involute has radius of curvature R' = s + p', and the derivative of its arc length (w.r.t. the arc length of the original curve) is $dS'/ds = R'\kappa$. Here p' is the initial length of 'unwrapped string'. Although there is always a point where R' = 0, there are no cusps, vertices or inflections.

Setting the starting parameter at the common point, the intrinsic equation for the involute is

$$2cS' = ac^2R'^2 + 2b(cR'\sin(c(R'-p')) + \cos(c(R'-p')) - \cos(cp')).$$
 (16)

3.3 Invariants

In his seminal work on intrinsic equations (Section IV/8), Cesàro [2] defines the *invariant* of a curve family as a function of the first k radii of curvature that is constant zero. In the general case, the invariant for our curves is

$$\rho^{3}(\rho_{(1)}\rho_{(4)} - \rho_{(2)}\rho_{(3)}) - 12\rho^{2}\rho_{(1)}^{2}\rho_{(3)} + 60\rho_{(1)}^{3}(\rho\rho_{(2)} - \rho_{(1)}^{2}). \tag{17}$$

When a = b we get a simpler expression:

$$\rho^2 \rho_{(3)} - 8\rho \rho_{(1)} \rho_{(2)} + 10\rho_{(1)}^3, \tag{18}$$

and also for the a=0 case:

$$\rho^2 \rho_{(3)} - 9\rho \rho_{(1)} \rho_{(2)} + 12\rho_{(1)}^3.$$

As a side note, for trig-aesthetic curves (Eq. 4) we have

$$\hat{c}^2 = \frac{3\rho^5 - 2\rho^3}{\rho_{(2)}},\tag{19}$$

and inserting this in the differential equation form (10) with a=0, b=1 and $c=1/\hat{c}$, we arrive at the invariant

$$\rho_{(2)}(\rho^3 - \rho) + \rho_{(1)}^2(2 - 3\rho^2), \tag{20}$$

depending only on ρ , $\rho_{(1)}$ and $\rho_{(2)}$. An even simpler expression uses the derivatives of curvatures:

$$\kappa \kappa'^2 + \kappa''(1 - \kappa^2). \tag{21}$$

3.4 Plotting

The Cartesian coordinates of the curves can be given by integrating the cosine and sine of the tangent angle. Assuming that the starting point is at the origin, and the starting angle is 0, we arrive at the (x, y) coordinates

$$\left(\int_0^s \cos\left(as + \frac{b}{c}\sin(cs)\right) \,\mathrm{d}s, \int_0^s \sin\left(as + \frac{b}{c}\sin(cs)\right) \,\mathrm{d}s\right),\tag{22}$$

which is, however, a non-trivial integral. Lehr cites Nielsen [6] to have converted such 'Lommel-integrals' to the solution of differential equations, and mentions their connection to Bessel functions, but in the end these did not provide a solution. Still, the dissertation contains many pages of exquisitely drawn curves (see Fig. 4) – how were these created?

Lehr plotted the integrands and used a *planimeter* (a mechanical tool for measuring the area inside a closed curve) to compute the integrals. Computations were carried out with the help of a *calculator* and a *slide-rule*. (See also Fig. 5.)

3.5 Analysis of subfamilies

In this section we will look at the characteristics of subfamilies. The classification is based on the relation between a and b, with a = b constituting the base form.

3.5.1 a = b

See Figure 4a (No. 15–24) for some examples. As discussed before, these curves have no inflections, just flat points, lying on a circle of radius $x_1/\sin\theta_1$. The remaining vertices are on

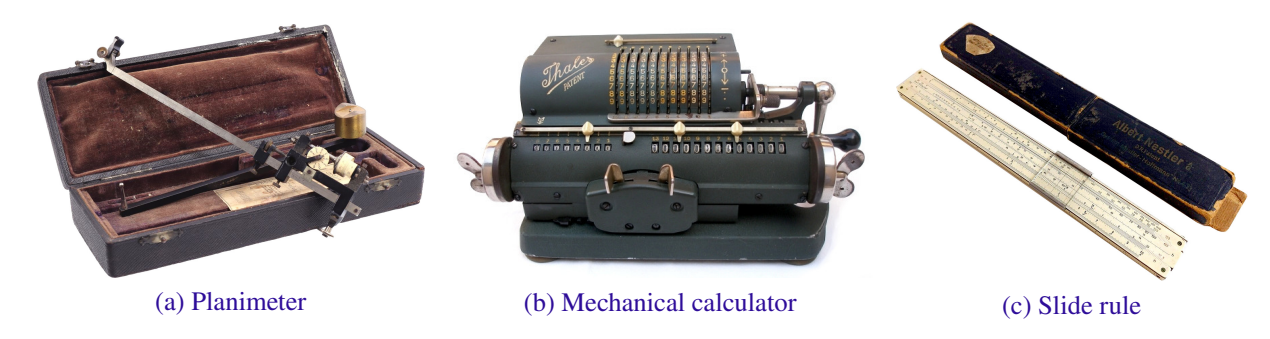


Fig. 5. Tools of the trade made in Germany in the 1930s.

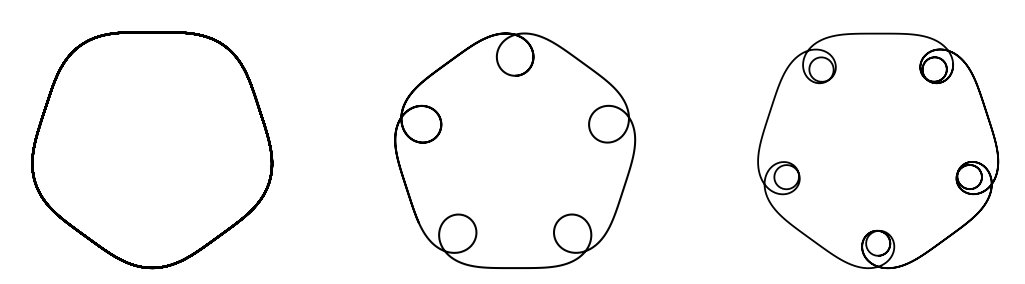


Fig. 6. Appearing loops with a = b $(\theta_1 = \frac{\pi}{5}, \frac{6\pi}{5}, \frac{11\pi}{5})$.

another circle (concentric with the first) with radius $x_1 \cot \theta_1 + y_1$. These circles degenerate to a pair of parallel lines when $\theta_1 = k\pi$ (e.g. No. 24). In this case a single period of the curve takes k full turns.

The curve is closed when θ_1 is a rational multiple of π , otherwise it goes on infinitely (e.g. No. 21). When $\theta_1 = (m + \frac{\nu}{n})\pi$, with ν and n relative prime and $\nu < n$, the shape is 'n-gonal', and makes $\mu = mn + \nu$ full turns, so e.g. for No. 16 n = 3, $\mu = 4$. As m grows, more and more extra loops appear, see Figure 6, and also Appendix A.

3.5.2 a > b

We will start from the base form a=b and start to increase the $\frac{a}{b}$ ratio to see how the curve reacts. For example with $\theta_1=\frac{\pi}{2}$, we get ellipse-like closed curves (No. 25–27 in Fig. 4a). There are two dotted ellipses in each of the figures: one has the same curvatures at the vertices, and the other has matching vertices (lying very close to the curve). As $\frac{a}{b}$ increases ($\frac{4}{3}$, 2 and 4 in these three figures) the curve more and more approaches the circle.

In the case of $\theta_1 = \pi$ the base case is a series of loops, and increasing $\frac{a}{b}$ pushes them closer together, thereby touching and intersecting each other, see Figure 7. Once again, the curve approaches a circle when $\frac{a}{b}$ goes to infinity.

In general, modifying θ_1 changes the shape according to the base form, while increasing $\frac{a}{b}$ makes the loops more circle-like and thus pushes them closer together.

3.5.3 a < b

As this is a very versatile part of the family, we divide it further in our analysis.

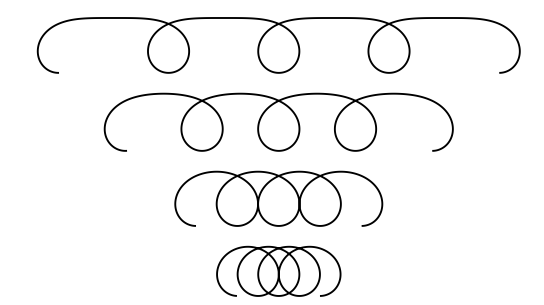


Fig. 7. Shrinking spring with $\theta_1 = \pi (\frac{a}{b} = 1, \frac{4}{3}, \frac{15}{7}, \frac{19}{5})$.

 $\theta_1 = 0 \ (a = 0)$. Let us first look at the subgroup $\theta_1 = 0$, which will serve as a basis for understanding the other forms.

In this case it would suffice to look at the $s \in [0, \frac{\pi}{2c}]$ interval because of its symmetry. The inflection point is at the center, i.e., $\bar{s} = \frac{\pi}{2c}$, and its tangent angle there is given by $\bar{\theta} = \frac{b}{c}$. From the boundary condition $\kappa_0 = a + b = 1$ we know that b = 1, so this class is the same as the trig-aesthetic curves, and $\bar{\theta} = \hat{c}$. Several examples are shown in Figure 1 with the associated shape parameters \hat{c} .

When $\bar{\theta} < \frac{\pi}{2}$, the curve looks like the wave

$$y = \rho_0 \tan^2 \bar{\theta} \cdot \left(1 - \cos \left(\frac{\cot \bar{\theta}}{\rho_0} x \right) \right), \tag{23}$$

which has the same vertex curvatures and inflectional tangent, but at the inflection point the wave curve has larger (x,y) coordinates and arc length than our curve, so both its amplitude and wavelength is larger. These deviations get larger and larger as $\bar{\theta}$ approaches $\frac{\pi}{2}$.

When $\bar{\theta}$ grows over $\frac{\pi}{2}$, the loops get more and more circular and more closely packed, first touching and then intersecting each other. First a loop touches the next one, then, for a larger $\bar{\theta}$ value, the one adjacent to that, and so on; in the end it simultaneously touches *all* other loops and becomes a closed curve when $\bar{\theta} \approx 2.4048$, the first zero of the Bessel function of the first kind J_0 . Its shape is similar to that of Bernoulli's lemniscate, although the latter has $\bar{\theta} = \frac{3\pi}{4} \approx 2.3562$ and is slightly more elongated.

As θ increases until π , the curve goes through the same process, but in the reverse order, touching and intersecting loops recede until they are separated, and we again get a wave-like form, but now there is an extra loop at the vertices.

For $\pi \leq \bar{\theta} \leq 2\pi$, the wave contracts and expands in the same way as before, except for the extra loops. The closed curve is obtained at $\bar{\theta} \approx 5.5201$, which is the second zero of J_0 (see Fig. 8). As one can imagine, the same things happen for $2\pi \leq \bar{\theta} \leq 3\pi$ etc., just with more extra loops. Note that the zeros of J_0 approach $\frac{3\pi}{4} + (n-1)\pi$, so the series of closed curves approaches Bernoulli's lemniscate.

In general we can also state that for $\bar{\theta} \leq \pi$ the curve resembles the *elastica*, see details in Section 3.6.

 $\theta_1 = \frac{\pi}{2} \ (a = \frac{c}{2})$. We start from the base form a = b, when the excess angle ϕ is 0, and start to increase ϕ (by decreasing a and c, and increasing b). The curve starts to narrow, taking on a biscuit-like shape, until its sides touch, and then intersect each other. Then we get back the base



Fig. 8. Lemniscate with loops ($\theta_1 = 0$, $\bar{\theta} \approx 5.5201$).

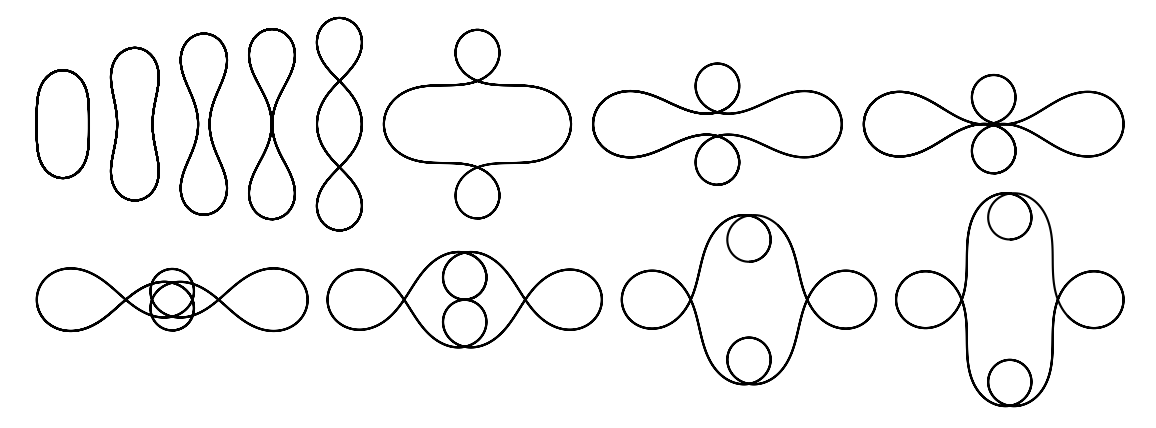


Fig. 9. The $\theta_1 = \frac{\pi}{2}$ family with growing ϕ value.

form rotated sideways, with two extra loops, see the top of Figure 9. From here on, the same process is repeated, creating two new loops, and so on.

 $\theta_1 = \pi \ (a = c)$. Starting from the base form $a = b \ (\phi = 0)$, the curve contracts and then expands as ϕ is increased, exactly like in the $\theta_1 = 0$ case, except for the extra loop that is already present in the base form. See also Figure 10 showing the contraction phase.

Generalization. The base form is defined by θ_1 . Increasing ϕ converts flat points into two inflection points and an arc with negative curvature between them, appearing as indentations or bulges. As these grow larger, the curve seems to contract, and individual parts of the curve touch, until eventually all vertices of a given type fall into the center of the curve. Then these vertices move farther away from the center, and vertices with the other curvature start to approach it. The process repeats as ϕ increases by π .

3.6 Comparison with elastic curves

The subfamily a=0 is very similar to the *elastica* family studied by Jacob Bernoulli and Euler. Since this has recently been also emphasized in a paper on trig-aesthetic curves [8], we will show the correspondences in notation.

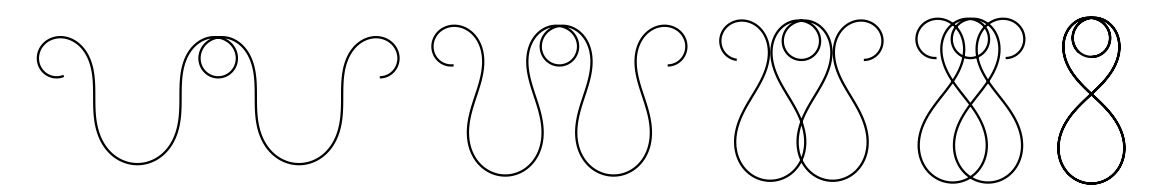


Fig. 10. The $\theta_1 = \pi$ family with growing ϕ value.

3.6.1 Elastica equations

Elastic curves have many definitions, based on pendulums, or the minimization of bending energy while retaining arc length. The one used by Lehr (following Bernoulli) is that the curvature at a given point is proportional to the distance from the line of force. Mathematically, taking the x axis as the line, and the proportional factor $-m^2$, this is described by the equation

$$\kappa = -m^2 y. (24)$$

Since $d\theta/ds = \kappa$ and $dy/ds = \sin \theta$, we obtain

$$\left(\frac{\mathrm{d}^2 y}{\mathrm{d}s^2}\right)^2 = \left(1 - \left(\frac{\mathrm{d}y}{\mathrm{d}s}\right)^2\right) m^4 y^2. \tag{25}$$

Now using v = dy/ds, we have

$$\left(v\frac{\mathrm{d}v}{\mathrm{d}y}\right)^2 = (1-v^2)m^4y^2,\tag{26}$$

and taking square root

$$\frac{\mathrm{d}v}{\mathrm{d}y} = \pm \frac{\sqrt{1 - v^2}m^2y}{v}.\tag{27}$$

Separating the variables and integrating, we get

$$\int \frac{v}{\sqrt{1-v^2}} \, \mathrm{d}v = \pm \int m^2 y \, \mathrm{d}y. \tag{28}$$

With $u=1-v^2$ (i.e., $v\,\mathrm{d} v=-\frac{1}{2}\mathrm{d} u$), this leads to

$$\int -\frac{1}{2\sqrt{u}} \, \mathrm{d}u = \pm \frac{m^2 y^2}{2} + C. \tag{29}$$

The integral of the left-hand side is just $-\sqrt{u} = -\sqrt{1-v^2}$ (plus an integration constant absorbed by C), so squaring both sides we obtain

$$1 - v^2 = \left(\frac{m^2 y^2}{2} + C\right)^2,\tag{30}$$

where C also absorbs the \pm sign. Finally this gives us

$$\frac{\mathrm{d}y}{\mathrm{d}s} = \sqrt{1 - \left(\frac{m^2 y^2}{2} + C\right)^2}.\tag{31}$$

(Lehr jumps directly from Eq. (25) to Eq. (31), as the intermediate steps are straightforward. . .) The above leads to an elliptic integral form of arc length:

$$s = \int_{y_0}^{y} \frac{\mathrm{d}y}{\sqrt{1 - \left(\frac{m^2 y^2}{2} + C\right)^2}}$$
 (32)

The intrinsic equation is then given by the use of the Jacobi elliptic function cn:

$$\kappa = m\sqrt{2(1-C)}\operatorname{cn}(ms). \tag{33}$$

Once again, this step is not trivial. Let us first formulate the differential equation for the elastic curve. Deriving Eq. (24)

$$\frac{\mathrm{d}^2 \theta}{\mathrm{d}s^2} = \frac{\mathrm{d}\kappa}{\mathrm{d}s} = -m^2 \frac{\mathrm{d}y}{\mathrm{d}s} = -m^2 \sin \theta,\tag{34}$$

so

$$\frac{\mathrm{d}^2}{\mathrm{d}s^2}\theta(s) + m^2\sin\theta(s) = 0. \tag{35}$$

Multiplying by $d\theta/ds$ and integrating it results in

$$\frac{1}{2}\kappa^2 - m^2\cos\theta = E,\tag{36}$$

where E is the integration constant. Its value is not arbitrary, however: from Eq. (31) we know that

$$\sqrt{1 - \cos^2 \theta} = \sin \theta = \frac{\mathrm{d}y}{\mathrm{d}s} = \sqrt{1 - \left(\frac{m^2 y^2}{2} + C\right)^2},\tag{37}$$

so $\cos\theta = \frac{m^2y^2}{2} + C$, and inserting it into Eq. (36) leads to

$$E = \frac{1}{2}(-m^2y)^2 - m^2\left(\frac{m^2y^2}{2} + C\right) = -m^2C,$$
(38)

so once again using Eq. (36) we obtain

$$\frac{\mathrm{d}\theta}{\mathrm{d}s} = \kappa = \pm m\sqrt{2(\cos\theta - C)}.\tag{39}$$

We can omit the sign as it will be absorbed by a constant later on. Separating the variables and integrating, assuming $s_0 = 0$, results in

$$s = \frac{1}{m\sqrt{2}} \int \frac{\mathrm{d}\theta}{\sqrt{\cos\theta - C}}.$$
 (40)

For convenience we change the variable to $\hat{\theta} = \frac{\theta}{2}$, using the fact that $\cos \theta = 1 - 2\sin^2 \frac{\theta}{2}$:

$$s = \frac{\sqrt{2}}{m\sqrt{1-C}} \int \frac{\mathrm{d}\hat{\theta}}{\sqrt{1-\frac{2}{1-C}\sin^2\hat{\theta}}} = \frac{\sqrt{2}}{m\sqrt{1-C}} \cdot F\left(\frac{\theta}{2}, \frac{2}{1-C}\right),\tag{41}$$

where F is the incomplete elliptic integral of the first kind. Here $k^2 = \frac{2}{1-C}$ is called the *parameter*, and k is the *modulus*. Denoting the value of the incomplete integral as u, we have

$$u = ms\sqrt{\frac{1-C}{2}} = \frac{ms}{k},\tag{42}$$

so $\frac{\theta}{2} = \operatorname{am}(u, k^2)$, the Jacobi amplitude. This means that

$$\cos\theta - C = 1 - 2\sin^2\frac{\theta}{2} - C = 1 - C - 2\sin^2(u, k^2) = 2\left(\frac{1}{k^2} - \sin^2(u, k^2)\right), (43)$$

SO

$$\kappa = 2m\sqrt{\frac{1}{k^2} - \sin^2(u, k^2)}. (44)$$

Since $dn^2(u, k^2) = 1 - k^2 sn^2(u, k^2)$, we arrive at

$$\kappa = \frac{2m}{k} dn(u, k^2) = m\sqrt{2(1-C)} dn(u, k^2).$$
(45)

Finally, using the relationship $dn(u, k^2) = cn(uk, 1/k^2)$, we at last obtain the expression

$$\kappa = m\sqrt{2(1-C)}\operatorname{cn}\left(ms, \frac{1-C}{2}\right). \tag{46}$$

We see that in this form the modulus is $\sqrt{\frac{1-C}{2}}$. The m parameter is essentially scaling the curve, and only C controls the shape. In the differential equation form (Eq. 35), when used with fixed boundary conditions $\theta(0) = 0$ and $\kappa(0) = 1$, the shape is controlled by $\lambda := m^2$.

By squaring Eq. (39) we get

$$\kappa^2 = 2m^2(\cos\theta - C),\tag{47}$$

which for the above mentioned boundary conditions gives

$$1 = 2m^2(1 - C),$$

leading to the relationship

$$\lambda = m^2 = \frac{1}{2(1 - C)}. (48)$$

3.6.2 Comparison

Note that the \hat{c} parameter of trig-aesthetic curves is the same as $\bar{\theta}$, when the latter is real. Refer to Figure 11 for a visual comparison: the associated numbers show the values of $\hat{c} = \bar{\theta} = \frac{1}{c}$ for trig-aesthetic, and of λ for elastica curves, with the boundary conditions $\theta(0) = 0$ and $\kappa(0) = 1$. For rows where $\lambda > \frac{1}{4}$, trig-aesthetic curves were selected based on visual similarity, but not necessarily with the same $\bar{\theta}$ value; the other examples are included to illustrate a variety of forms.

Lehr divides the family into classes based on the value of the C integration constant, each exhibiting a distinct shape type:

• C=1 ($\lambda=\infty, \bar{\theta}=0$): both curves degenerate to a line.

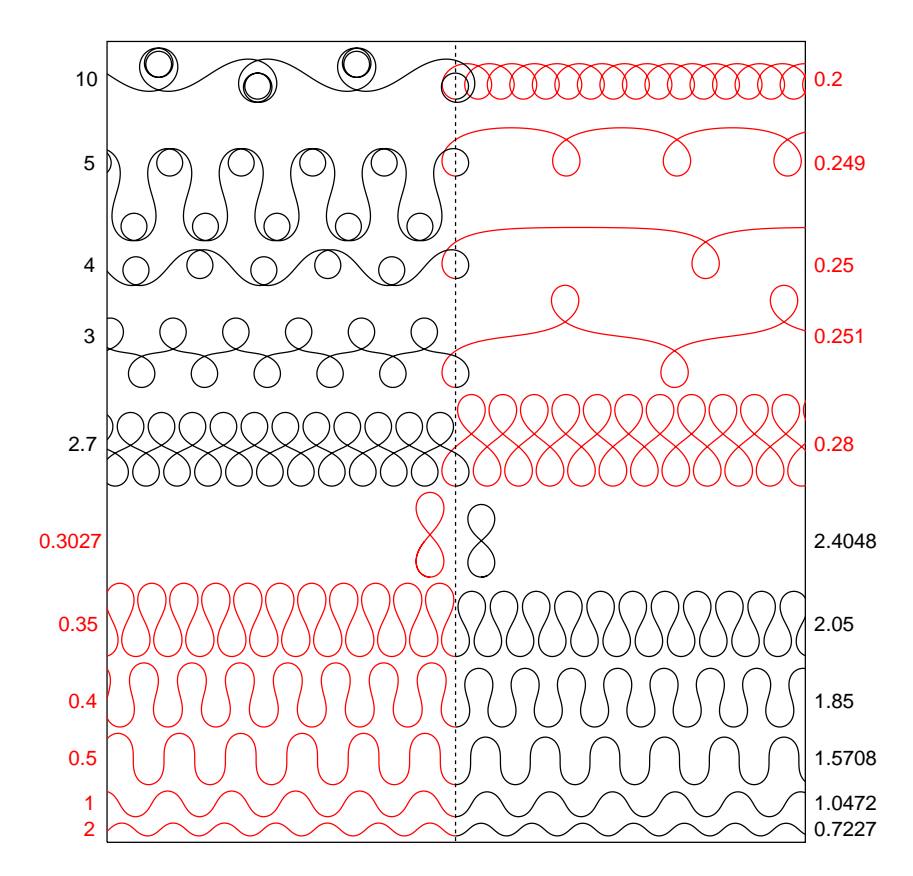


Fig. 11. Comparison of trig-aesthetic curves (black) and elastica (red) [8].

- 0 < C < 1 $(\frac{1}{2} < \lambda < \infty, 0 < \overline{\theta} < \frac{\pi}{2})$: both are similar to sine waves; vertex curvature is ± 1 for both, but the amplitude and wavelength is smaller for trig-aesthetic curves.
- C=0 ($\lambda=\frac{1}{2},\ \bar{\theta}=\frac{\pi}{2}$): Lehr states that this is the only elastic curve that is also a Ribaucour curve (with factor 2), i.e., the radius of curvature is proportional to the normal directional distance to a given line. This seems not to be the case: here the curvature (and not the *radius* of curvature) is proportional to the normal distance.
- -1 < C < 0 $(\frac{1}{4} < \lambda < \frac{1}{2}, \frac{\pi}{2} < \bar{\theta} < \pi)$: we further divide into 3 cases below.
 - $\bar{x} > 0$: both curves touch, contract and intersect themselves, the difference in amplitude is more and more visible.
 - $\bar{x}=0$: Bernoulli's lemniscate is an intermediate form between the two, as can be seen from the values of $\bar{\theta}$ (elastica: $\approx 130^{\circ}42'$, lemniscate: 135° , trig-aesthetic: $\approx 137^{\circ}47'13''$).
 - $\bar{x} < 0$: the loops start to separate, much faster for the elastica than for trig-aesthetic curves.
- C=-1 ($\lambda=\frac{1}{4}, \bar{\theta}=\pi$): from here on, the two curves have no connection. In this special case the elastica has the closed form

$$\left(-\frac{2}{m}\sin\frac{\theta}{2} + \frac{1}{m}\ln\tan\left(\frac{\theta}{4} + \frac{\pi}{4}\right), \frac{2}{m}\left(1 - \cos\frac{\theta}{2}\right)\right). \tag{49}$$

- $-\infty < C < -1$ ($0 < \lambda < \frac{1}{4}$, $\bar{\theta}$ imaginary): the elastica takes on an ever-contracting spring-like form, while the trig-aesthetic curve ($\pi < \hat{c} < \infty$) goes through contractions and expansions as explained in Section 3.5.
- $C = -\infty$ ($\lambda = 0$, $\bar{\theta}$ imaginary): corresponds to the case $\hat{c} = \infty$; both curves are circles.

3.7 Space curves

As a generalization to 3D space, we can add a constraint on the radius of torsion τ , similarly to Eq. (5):

$$\frac{1}{\tau} = \alpha + \beta \cos(\gamma s + \delta). \tag{50}$$

But the Frenet equations can only be integrated easily when $\delta=0, c=\gamma$, and $\alpha\beta-ab=0$, i.e.,

$$\frac{1}{\rho} = a + b\cos(cs), \qquad \qquad \frac{1}{\tau} = \alpha + \frac{ab}{\alpha}\cos(cs). \tag{51}$$

These are all helices that can be constructed on a cylinder whose normal section is a curve of Eq. (5).

Since this line of generalization does not seem to be very fruitful, Lehr turns to curves defined on the sphere with geodesic curvature

$$\kappa_g = \frac{1}{\rho_g} = a + b\cos(cs). \tag{52}$$

Since $\kappa^2 = \kappa_g^2 + \kappa_n^2$, and the normal curvature κ_n on a sphere of radius R is $\frac{1}{R}$, we have

$$\frac{1}{\rho} = \sqrt{(a + b\cos(cs))^2 + \frac{1}{R^2}}, \qquad \frac{1}{\tau} = \frac{Rbc\sin(cs)}{R^2(a + b\cos(cs))^2 + 1}.$$
 (53)

If R goes to infinity, the torsion approaches zero and we get back our original curves. Otherwise this leads to a complex Riccati differential equation, but we can make some general remarks.

- The curves are periodic with period $\frac{2\pi}{c}$.
- The curvature is always positive, and maximal at the endpoints.
- The minimal value of (ordinary or geodesic) curvature is at the midpoint $s = \frac{\pi}{c}$, where the torsion is zero.
- The geodesic curvature becomes zero when $\cos(cs) = -\frac{a}{b}$ (occurs for two values when a < b, symmetric to the midpoint).

For easier analysis and plotting, Lehr uses stereographic projection onto the equatorial plane (see Fig. 4b). For a spherical point (x, y, z) the projection is

$$(\xi, \eta) = \frac{R}{R - z}(x, y),\tag{54}$$

while the inverse projection is

$$(x,y,z) = \frac{1}{\xi^2 + \eta^2 + R^2} (2R^2\xi, 2R^2\eta, R(\xi^2 + \eta^2 - R^2)).$$
 (55)

A circle around a projected point (ξ_0, η_0) with radius ρ_0 is also a circle on the sphere in the plane

$$Ax + By + Cz + D = 0 ag{56}$$

with A:B:C:D being

$$2R\xi_0: 2R\eta_0: \xi_0^2 + \eta_0^2 - \rho_0^2 - R^2: -R(\xi_0^2 + \eta_0^2 - \rho_0^2 + R^2).$$
 (57)

Then the radius of the 3D circle ρ depends on the distance δ of the plane from the center $(\rho^2 = R^2 - \delta^2)$. Consequently:

$$\rho^2 = \frac{4R^4\rho_0^2}{(\xi_0^2 + \eta_0^2 - \rho_0^2 - R^2)^2 + 4R^2(\xi_0^2 + \eta_0^2)}.$$
 (58)

If we now look at a circle going through (ξ^*, η^*) with tangent angle t^* (measured from the positive ξ axis), we get

$$\xi_0 = \xi^* \pm \rho_0 \sin t^*, \qquad \eta_0 = \eta^* \mp \rho_0 \cos t^*,$$
 (59)

so if we introduce $d^2 = \xi^{*2} + \eta^{*2}$ for the squared distance of the point from the origin, and $c = \pm \xi^* \sin t^* \mp \eta^* \cos t^*$ for the signed distance of the origin from the tangent line, we arrive at

$$\rho^2 = \frac{4R^4 \rho_0^2}{(d^2 + 2\rho_0 c - R^2)^2 + 4R^2(d^2 + \rho_0^2 + 2\rho_0 c)},$$
(60)

and then

$$\rho_0 = \frac{(d^2 + R^2)\rho}{2(R\delta - c\rho)} = \frac{d^2 + R^2}{2(e - c)},\tag{61}$$

with $e = \frac{R\delta}{\rho}$.

For a spherical curve with known geodesic curvature, the curvature circle is obtained by intersecting the sphere with the osculating plane. From this we can compute the curvature circle in the plane, whose radius gives the radius of curvature for the projected curve (note that with ρ being the radius of curvature, we have $e = \frac{R^2}{\rho_g}$). Now we have all information to plot the 2D image of the curve.

Let us take example No. 31 in Figure 4a (a trig-aesthetic curve with $\hat{c}=\frac{11}{14}$), and create its geodesic curvature version on a large sphere. The resulting curve is very similar (see Fig. 4b, No. 89, $\rho_g(0)/R=0.4$). As we reduce the sphere's radius, the vertices approach each other, and then separate again (No. 90–94, $\rho_g(0)/R=1,1.2,1.37,1.4,2$). The curve can also close on itself, as shown in No. 95 ($\rho_g(0)/R=2.94$). As R approaches 0, the curve approximates a great circle of the sphere.

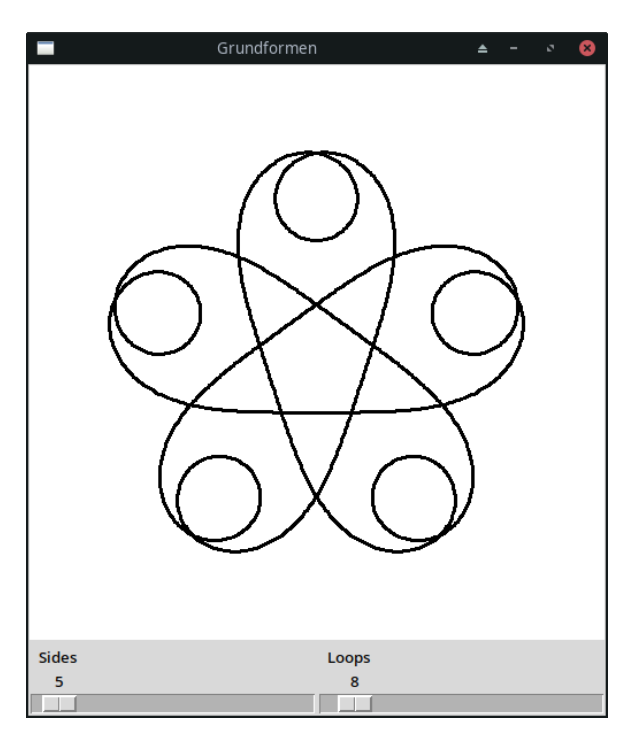


Fig. 12. Applet for experimenting with base forms.

4 Conclusion

Eduard Lehr described the curve family defined by Eq. (5), investigating the parameters' effect on its different shapes, including the *base forms* and what are now called *trig-aesthetic curves*. Notes on derived curves (evolute, offset and involute) were supplied. A comparison to Euler's *elastica* was also included, as well as preliminary work on generalization to space curves, particularly to spherical curves.

In this work we have aimed to extract the most interesting parts from Lehr's dissertation, and also supplemented it in several places, notably on the derivation of the elastic curve, and by the addition of a figure comparing it to trig-aesthetic curves. Several errors in the equations were corrected, and some biographical background on Lehr was also included for completeness.

Acknowledgements

This project has been supported by the Hungarian Scientific Research Fund (OTKA, No. 145970). The author would like to thank the Max-Planck-Gymnasium München, the Bavarian State Archives, the Military Archives of the Federal Archives of Germany, and the Library and Archives of the Technical University of Munich for providing biographical data on Eduard Lehr.

Appendix A Applet for exploring base forms

The TCL/TK applet in Figure 12 is a convenient tool for plotting different base forms; it can also be easily modified to investigate other curves. Here a=b=1 and $c=n_{\rm sides}/n_{\rm loops}=n/\mu$. The source code is shown in Figure 13.

```
lassign \{500\ 3\ 200\} size lineWidth resolution; # params lassign \{5\ 8\} sides loops
wm title . "Grundformen'
canvas .canvas -width $size -height $size -bg white
scale .f.sides -variable sides -from 1 -to 100 -label Sides -orient horizontal -command redraw
scale .f.loops -variable loops -from 1 -to 100 -label Loops -orient horizontal -command redraw
pack .f.sides .f.loops -side left -expand 1 -fill x
pack .canvas .f -fill x
proc redraw args {
    global resolution loops size lineWidth
     .canvas delete all
    set res [expr {\text{sresolution*}}] set smax [expr {2*}scops*acos(-1)}] lassign {\{0\ 0\}} {0\ 0} {0\ 0} p bbmin bbmax s1
     set points [list $p]
     for {set i 0} {$i < $res} {incr i} {
         set s [expr {$smax*$i/($res-1.0)}]
         set d [list [integrate fx $s1 $s] [integrate fy $s1 $s]]
         set p [add $p $d]
         set bbmin [vmin $p $bbmin]
         set bbmax [vmax $p $bbmax]
         lappend points $p
         set s1 $s
    set scale [expr {$size/[distance $bbmin $bbmax]}]
    set center [mul [add $bbmin $bbmax] -0.5]
set offset [list [expr {$size/2}]] [expr {$size/2}]]
     set coords {}
     foreach p $points {
         lappend coords {*}[add [mul [add $p $center] $scale] $offset]
     .canvas create line $coords -width $lineWidth
proc vmin {u v} {
    list [expr {min([lindex $u 0],[lindex $v 0])}] [expr {min([lindex $u 1],[lindex $v 1])}]
proc vmax {u v} {
    list [expr {max([lindex $u 0],[lindex $v 0])}] [expr {max([lindex $u 1],[lindex $v 1])}]
proc add {u v} {
    list [expr {[lindex $u 0]+[lindex $v 0]}] [expr {[lindex $u 1]+[lindex $v 1]}]
proc mul {u x} {list [expr {[lindex $u 0]*$x}] [expr {[lindex $u 1]*$x}]} proc sub {u v} {add $u [mul $v -1]} proc dot {u v} {expr {[lindex $u 0]*[lindex $v 0] +
                           [lindex $u 1]*[lindex $v 1]}}
proc norm u {expr {sqrt([dot $u $u])}}
proc distance {p q} {norm [sub $p $q]}
proc theta {s} {
    global sides loops
    set c [expr {($sides+0.0)/$loops}]
expr {$s+1/$c*sin($c*$s)}
proc fx {s} {expr {cos([theta $s])}}
proc fy {s} {expr {-sin([theta $s])}}
proc integrate {f a b} {
    set x {-0.906179845937 -0.538469310107 0 0.538469310107 0.906179845937}
     set w {0.236926885057 0.478628670499 0.568888888889 0.478628670499 0.236926885057}
    set sum 0
     set m [expr {($a+$b)/2}]
     for {set i 0} {$i < 5} {incr i} {</pre>
         set xi [expr {($b-$a)/2*[lindex $x $i]+$m}]
set sum [expr {$sum+[lindex $w $i]*[$f $xi]}]
    expr {\$sum*(\$b-\$a)/2}
redraw
```

Fig. 13. TCL/TK source for the applet in Fig. 12.

References

- [1] ABBENA, E., SALAMON, S., GRAY, A. *Modern Differential Geometry of Curves and Surfaces with Mathematica*. Chapman and Hall/CRC, third edition, 2017.
- [2] CESÀRO, E. Lezioni di geometria intrinseca. Naples, 1896.
- [3] LEHR, E. Über die Kurven, deren Krümmung eine periodische Funktion des Bogens ist. Ph.D. thesis, Technische Hochschule München, 1932.
- [4] LEOPOLD, L. B., LANGBEIN, W. B. River meanders. *Scientific American*, volume 214, no. 6, 1966: pages 60–73.
- [5] MIURA, K. T., GOBITHAASAN, R. U. Log-aesthetic curves and similarity geometry. *International Journal of Automation Technology*, volume 18, 2024: pages 591–602, doi: 10.20965/ijat.2024.p0591.
- [6] NIELSEN, N. Handbuch der Theorie der Cylinderfunktionen. B. G. Teubner, 1904.
- [7] North Dakota State University & AMS. Eduard Lehr Mathematics Genealogy Project. https://mathgenealogy.org/id.php?id=65765, accessed: March 2025.
- [8] SALVI, P. Generalized catenaries and trig-aesthetic curves. *Computer-Aided Design and Applications*, volume 23, no. 1, 2026: pages 56–67, doi:10.14733/cadaps.2026.56-67.
- [9] WOLFRAM, S. A New Kind of Science. Wolfram Media, 2002.

Péter Salvi

Department of Control Engineering and Information Technology Budapest University of Technology and Economics Műegyetem rkp. 3., H-1111 Budapest, Hungary e-mail: salvi@iit.bme.hu

MST-based clustering for curve and surface reconstruction

Šárka Voráčová

Abstrakt

Problém minimálneho kostrového stromu (MST) bol v literatúre spomenutý už v roku 1926, čo z neho robí jeden z najstarších a najdôkladnejšie skúmaných problémov v oblasti výpočtovej geometrie. Okrem svojho trvalého teoretického a algoritmického významu má MST široké uplatnenie pri riešení mnohých praktických úloh analýzy dát, ako aj pri segmentácii obrazu a rekonštrukcii kriviek a plôch.

V tomto článku predstavujeme metódy na rekonštrukciu kriviek a plôch pomocou algoritmu euklidovského MST, ktorý môže zabezpečiť, že rekonštruovaná krivka bude efektívna z hľadiska konektivity a vzdialenosti.

Kľúčové slová: euklidovský minimálny kostrový strom, rekonštrukcia kriviek, rekonštrukcia plôch, zhlukovanie

Abstract

The Minimum Spanning Tree problem has been referenced in the literature as early as 1926, making it one of the oldest and most thoroughly studied problems computational geometry. Alongside enduring theoretical and algorithmic appeal, MST is valuable for addressing numerous practical data analysis problems as segmentation image reconstruction of the curve and surfaces. In this paper, we present curve and surface reconstruction methods using the Euclidean MST algorithm. The MST can help ensure that the reconstructed curve is efficient in terms of connectivity and distance.

Keywords: Euclidean minimum spanning tree, curve reconstruction, surface reconstruction, clustering

1 Introduction

The Euclidean minimum spanning tree (EMST) problem has applications in many fields, and many efficient algorithms have been developed to solve it. With references in the literature as early as 1926, the minimum spanning tree (MST) problem is one of the oldest and most thoroughly studied problems in computational geometry. In addition to this long-standing theoretical and algorithmic interest, the MST is useful for many practical data analysis problems. Many optimization problems can be posed in the search for the MST in a network. The MST is also used as an approximation for the traveling salesman problem [4], in document clustering, mesh generation [11], and curve and surface reconstruction [13], [15].

MST of the graph connects all the vertices, without any cycles and with the minimum possible total edge weight. EMST can be found as the minimum spanning tree of a complete graph with the points as vertices and the Euclidean distances between points as edge weights.

The problem of MST was first published in 1926 by Otakar Borůvka in the paper "O jistém problému minimálním" [5] as a method of constructing an efficient electricity network for

Moravia. This algorithm is often referred to as Sollin's algorithm, particularly in the context of parallel computing literature [16]. Borůvka's algorithm is well-suited for parallelization, as the selection of minimum-weight edges for each component can be done independently.

The standard procedure, known as Prim's algorithm, was formulated by the eminent number theorist Vojtěch Jarník in response to Borůvka's work [12], [16].

Finding the nearest neighbor of components in a spanning forest is the computational bottleneck in both traditional MST algorithms like Kruskal's and Prim's and more advanced methods [1], [3], [6]. Borůvka's algorithms require at most log V steps and a running time of $O(E \log V)$, where E is the number of edges and V is the number of vertices. Variants for planar graphs work with linear time complexity.

2 Euclidean Minimum Spanning Tree

Computing the Euclidean Minimum Spanning Tree (EMST) is a classic problem in computational geometry. Similar to the MST, it is utilized in various applications such as clustering, pattern classification, surface reconstruction, TSP approximations, and computer graphics.

The edges of the minimum spanning tree meet at angles of at least 60°, with equality only when they form two sides of an equilateral triangle. This is because, for two edges forming any sharper angle, one of the two edges could be replaced by the third, shorter edge of the triangle they form, forming a tree with a smaller total length. Euclidean minimum spanning tree is a subgraph of other geometric graphs including the relative neighborhood graph and Delaunay triangulation. By constructing the Delaunay triangulation and then applying a graph minimum spanning tree algorithm, the minimum spanning tree of given planar points may be found in linear time.

Traditional EMST methods scale quadratically, and many advanced algorithms have been created to solve the problem on general graphs. Fredman and Tarjan [7] demonstrated a bound of $O(E \log V)$ for V points and E edges by using Jarník's algorithm with the Fibonacci heap data structure. However, these general algorithms are not suitable for large problems because they depend linearly on the number of edges. In the case of Euclidean graphs, the edge set consists of all pairs of points. Thus, linear scaling in E corresponds to quadratic scaling in the number of points V, necessitating the consideration of alternative approaches.

Shamos & Hoey [17] applied the Voronoi diagram to constructing the MST in the Euclidean plane. The Voronoi diagram can be constructed in $O(V \log V)$ time and contains O(V) edges. Since the MST is a subset of the edges in the dual of the Voronoi diagram, the MST can be found in $O(V \log V)$ time using one of the algorithms above. Agarwal et al. [1] showed that the EMST problem is linked to solving bichromatic closest pairs for specific subsets of the input set. The bichromatic closest pair problem is defined as follows: given two sets of points, one red and one green, the task is to find the red-green pair with the minimum distance between them. By employing a geometric approach that leverages well-separated pair decomposition (WSPD), it is possible to efficiently achieve a time complexity of $O(V \log V)$ when constructing the EMST in a three-dimensional space.

3 MST-based Clustering

Minimum Spanning Tree-based clustering is an unsupervised machine learning technique that identifies clusters by leveraging graph theory. It constructs an MST from a given dataset's distance graph and removes edges that exceed a certain threshold to create distinct clusters. In the clustering literature, this is often referred to as single-linkage clustering. The definition of inconsistent edges is a major issue that has to be addressed in all MST-based clustering algorithms.

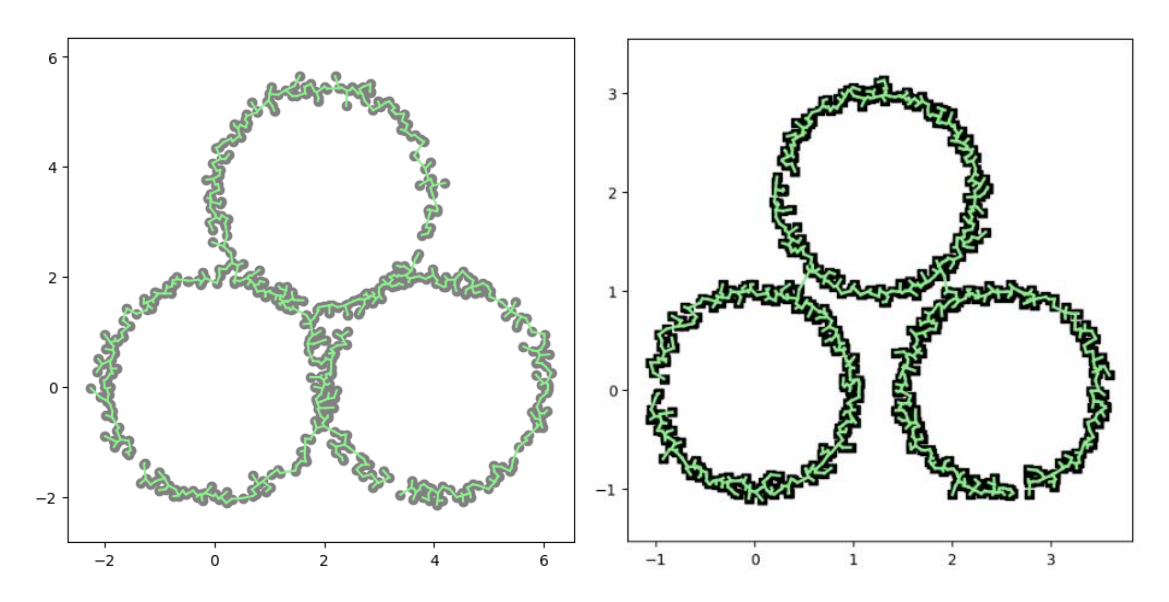


Fig. 1. Example dataset and their Euclidean minimum spanning trees. MSTs often lead to representations of well-separable clusters of arbitrary shapes.

This method was described in the 1970s [2], and recent advancements in MST-based clustering have led to the development of various innovative algorithms and methodologies [9]. In 1969 Gower and Ross [10] showed the equivalence between the naive clustering algorithm and Kruskal's algorithm for minimum spanning trees. How well particular MST-based methods perform in general and whether they are competitive relative to other popular clustering procedures is still an open problem [9].

In practice, many algorithms construct simpler representations (samples) of the search space to make the identification of clusters more tractable. For instance, in the well-known K-means algorithm by Lloyd, we iteratively seek k cluster centroids so that a point's cluster belongingness can be determined through the proximity thereto. By contrast, the second most famous algorithm Density-Based Spatial Clustering of Applications with Noise (DBSCAN) identifies clusters based on density, grouping points with sufficient neighbors while marking outliers [7]. It does not require specifying the number of clusters and excels in detecting arbitrarily shaped clusters (Fig. 2).

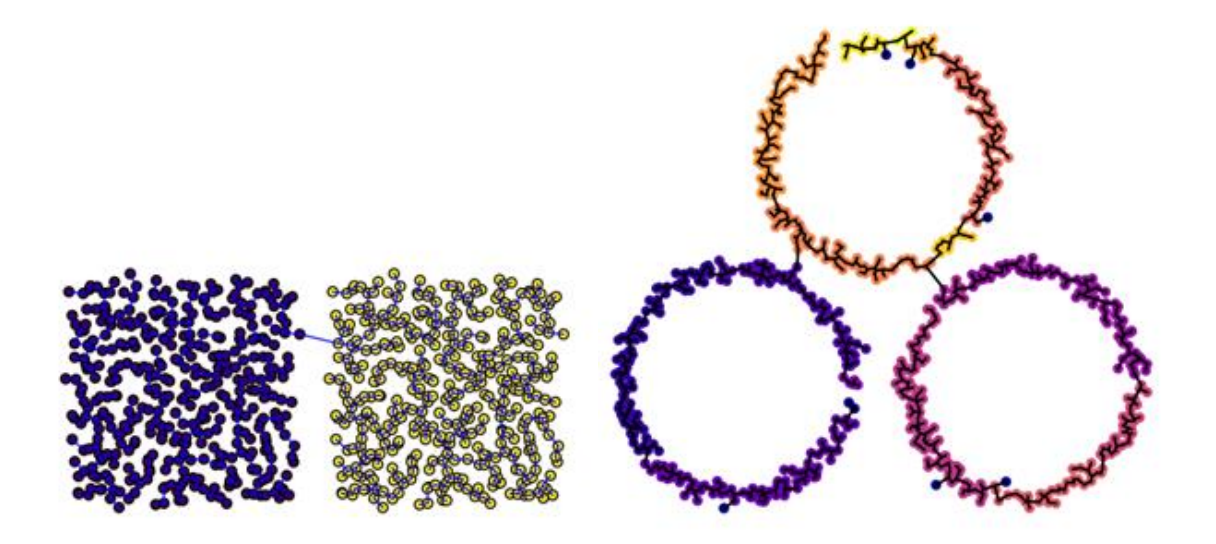


Fig. 2. Left: Distinct points on well-sampled two squares were safely distinguished, the edge length criterion for MST-based clustering can be safely set.

Right: A relatively good sample of three circles correctly distinguished MST-based clustering, in contrast, DBSCAN incorrectly separated the points of the circles.

4 Curve Reconstruction

Our goal is to apply EMST to a point cloud and test the curve reconstruction capabilities of this method for different types of data. Curve reconstruction entails creating a continuous curve that accurately represents a given set of points. The main problem is to correctly distinguish sets of points belonging to different continuous parts of curves, to divide the point cloud into individual clusters. Cluster analysis deals with this problem and motivated our choice of minimal spanning trees as shape descriptors for curves.

The algorithm for curve reconstruction using MST can be delineated into four steps:

- 1. Complete weighted graph: Create a complete graph where each point is a node, and the edges represent the pairwise distances. This involves using Euclidean distance or any other suitable distance metric that is relevant to the data.
- 2. Minimum Spanning Tree on the complete graph.
- 3. Path Extraction from MST: This involves starting from an arbitrary point and traversing the MST to create a sequence of points.
- 4. Curve Interpolation: The points can be further smoothed or interpolated to get a continuous curve. Techniques such as spline interpolation (for example B-splines) or piecewise linear interpolation can be applied to generate a smooth curve from the discrete points obtained from the MST.

In our algorithm, we combine the EMST approach with the statistical method for local approximation using the moving squares method. To prevent the effects of unwanted points in the local regressions, we need to make a certain structure (as simple as possible) for the point set to define the connectivity of the point elements. We calculate the average edge length (μ) and standard deviation (σ) of the edge lengths. Then the tree was pruned by removing all edges longer than $\mu + k\sigma$, where k is a suitable constant. The choice of k affects the level of detail in

the reconstruction. A smaller k preserves more details but may introduce noise, while a larger k produces a smoother but less detailed reconstruction.

The next step is to separate the components of the graphs representing the different curves:

- 1. Identify the endpoints: Vertices with degree 1 in the pruned EMST.
- 2. Traverse the pruned EMST: Start from an arbitrary endpoint and follow the edges, always choosing the edge that forms the smallest angle with the previous edge. If a junction (a vertex with degree > 2) is encountered, choose the edge that forms the smallest angle. Continue until reaching another endpoint or return to the starting point.
- 3. Handle branching: Connect appropriate branches at junction points. In the case of closed curves, it may be necessary to connect the last point to the first point if they are close.
- 4. Smooth the reconstructed curve (optional).

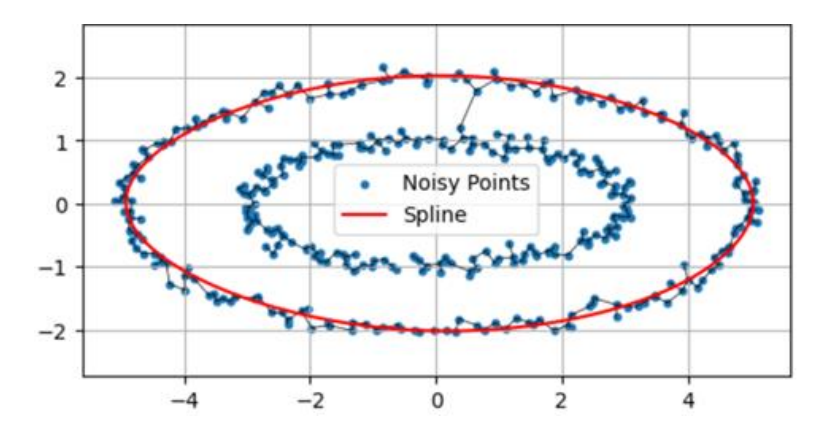


Fig. 3. Enhanced Minimum Spanning Tree from Noisy Points.

5 Surface Reconstruction

Cluster analysis is essential for 3D reconstruction, especially in organizing and segmenting point cloud data gathered from laser scanning, photogrammetry, or depth sensors. By grouping points based on their spatial proximity and geometric similarity, clustering helps to identify significant structures, filter out noise, and enhance surface reconstruction processes.

For the segmentation of 3D point cloud data, we applied the same clustering algorithms as those used in planar analysis. Our experiments demonstrated comparable segmentation performance using K-Means and DBSCAN, with both methods successfully identifying distinct surface regions. The effectiveness of clustering in 3D reconstruction was strongly influenced by the density of sampled points, as well as the levels of noise.

Our reconstruction of a 3D surface from a point cloud is largely dependent on the integration of the Minimum Spanning Tree (MST) methodology, which is applied to identify contiguous regions and surface texture. The use of geometric and graph-based approaches improves the creation of optimized networks that emphasize both geometric accuracy and computational efficiency.

29

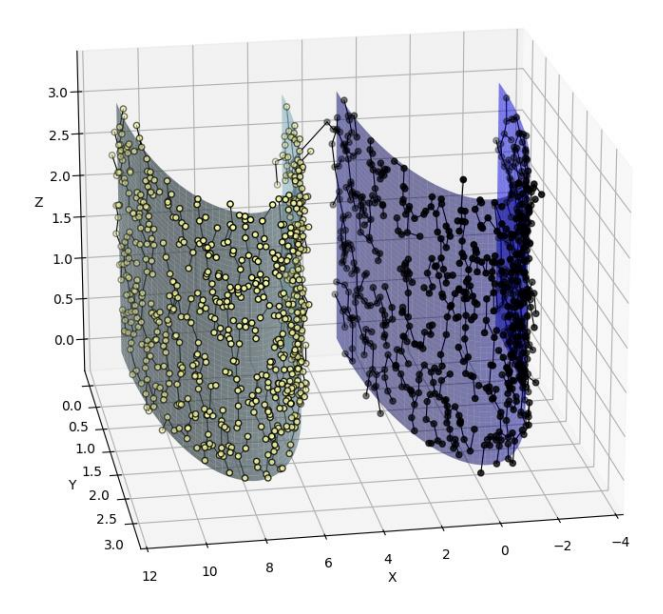


Fig. 4. A good sample of points from two cylindrical surfaces sufficiently far apart is correctly separated by both EMST and k-means clustering for k = 2.

In this study, we compared MST-based clustering with traditional methods such as K-Means and DBSCAN. To ensure a comprehensive evaluation, we generated synthetic datasets enriched with varying levels of noise and assessed clustering performance on samples representing segments of cylindrical surfaces, spheres, and planes in different spatial configurations. The analysis focused on the ability of each method to accurately capture cluster structures under varying noise conditions and geometric complexities. Our findings provide insights into the strengths and limitations of MST-based clustering relative to density-based and centroid-based approaches in complex spatial distributions.

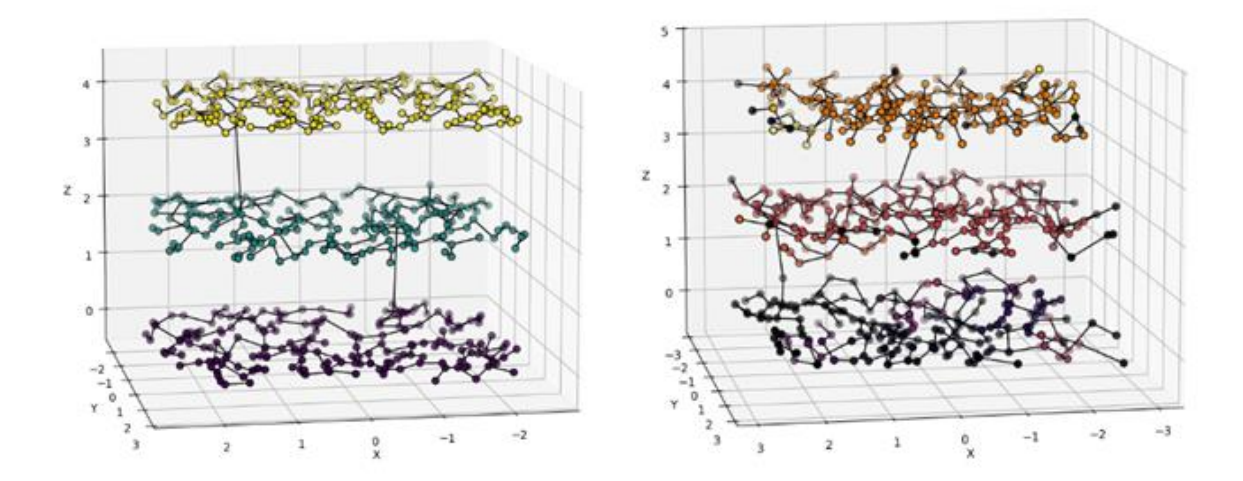


Fig. 5. Color-coded DBSCAN results for the low-noise sample and the higher-noise, unevenly sampled points. For both samples, MST-based clustering accurately identified points belonging to the three planes, whereas DBSCAN's resulting coloring was less precise.

Note. MST is used in triangulation mainly as an initial step or as part of more complex algorithms [15]. The basic idea is that the Minimum Spanning Tree (MST) provides a skeleton for triangulation, capturing the key connections between points. The procedure can be simplified into three main steps. First, an MST is constructed for a given set of points. Next, additional edges are added to the MST to form a triangulation. Finally, the triangulation is optimized, for example, by applying the Delaunay criterion to improve its properties.

6 Conclusion

The use of the Minimum Spanning Tree (MST) for curve and surface reconstruction offers several advantages, particularly in capturing complex, non-uniform structures. Unlike centroid-based methods such as K-Means, MST-based clustering does not require predefined cluster counts and can adapt to varying point densities. This makes it particularly effective for reconstructing irregular surfaces and handling topological continuity. In our experiments, MST-based clustering achieved successful segmentation in 79% of cases, even when samples were intentionally degraded with varying levels of noise. This demonstrates its robustness in scenarios where data completeness and uniformity are compromised. Additionally, MST naturally preserves geometric connectivity, making it well-suited for reconstructing continuous features in scattered point clouds.

However, MST-based approaches also present limitations. The computational complexity of constructing an MST can be higher than that of K-Means, especially for large-scale datasets. Moreover, MST methods can be sensitive to outliers, which may create artificial connections between unrelated points. In our study, K-Means achieved the highest segmentation success rate (85%), but only when the number of clusters was manually specified. In contrast, DBSCAN performed the worst (53%), likely due to its reliance on density thresholds, which struggled with non-uniformly sampled surfaces. These results highlight the strengths of MST in adaptive clustering while also underscoring its challenges in handling noise and scalability compared to established clustering techniques.

The utilization of Minimum Spanning Trees (MST) in triangulation processes offers several notable benefits. MST provides a solid starting point for establishing connections between data points, laying the groundwork for further triangulation refinement. Triangulations derived from MST often result in configurations with shorter overall edge lengths, although the MST alone does not guarantee an optimal solution. It proves to be a valuable initial step, potentially requiring further optimization to achieve the desired results. MST is instrumental in revealing underlying structures within datasets by highlighting key connections, aiding in pattern recognition, and facilitating cluster identification.

References

- [1] AGARWAL, P. K., EDELSBRUNNER, H., SCHWARZKOPF, O. a WELZL, E., Euclidean minimum spanning trees and bichromatic closest pairs. Discrete & Computational Geometry, 1991, roč. 6, č. 3, pp. 407–422.
- [2] ARKADEV, A. G. a BRAVERMAN, E. M., *Computers and Pattern Recognition. Washington*, D.C.: Thompson Book Co, 1967.
- [3] ARYA, S. a MOUNT, D. M., A fast and simple algorithm for computing approximate Euclidean minimum spanning trees. In *Symposium on Discrete Algorithms*, pp. 1220–1233, 2016.

- [4] ARORA, S., Polynomial time approximation schemes for Euclidean traveling salesman and other geometric problems. In *Journal of the ACM*, 1998, roč. 45, č. 5, pp. 753–782.
- [5] BORŮVKA, O., O jistém problému minimálním. In *Acta Societatis Scientiarium Naturalium Moravicae*, 1926. roč. 3, s. 37–58.
- [6] EPPSTEIN, D., Finding relevant points for Nearest-Neighbor classification. In *Society for Industrial and Applied Mathematics eBooks*, 2022, pp. 68–78.
- [7] ESTER, M., KRIEGEL, H. P., SANDER, J. a XU, X., A density-based algorithm for discovering clusters in large spatial databases with noise. In *Proceedings of the Second International Conference on Knowledge Discovery and Data Mining* (KDD'96). AAAI Press, pp. 226–231, 1996.
- [8] FREDMAN, M. a TARJAN, R., Fibonacci heaps and their uses in improved network optimization algorithms. In *Journal of the ACM*. 1987, roč. 34, č. 3, pp. 596–615.
- [9] GAGOLEWSKI, M., CENA, A., BARTOSZUK, M. et al., Clustering with Minimum Spanning Trees: How Good Can It Be? In *Journal of Classification*, 2024.
- [10] GOWER, J. C. a ROSS, G. J., Minimum spanning trees and single linkage cluster analysis. In *Journal of the Royal Statistical Society*, Series C. 1969, roč. 18, č. 1, pp. 54–64.
- [11] ITIER, V., TOURNIER, N., PUECH, W., SUBSOL, G. a PEDEBOY, J., Analysis of an EMST-based path for 3D meshes. In *Computer-Aided Design*. 2015, roč. 64, pp. 22–32.
- [12] JARNÍK, V., O jistém problému minimálním. (Z dopisu panu O. Borůvkovi). In *Acta Societatis Scientiarium Naturalium Moravicae*. 1930, roč. 6, s. 57–63.
- [13] LEE, I., Curve reconstruction from unorganized points. In *Computer Aided Geometric Design*. 2000, roč. 17, č. 2, pp. 161–177.
- [14] MARCH, W. B., RAM, P. a GRAY, A. G., Fast Euclidean minimum spanning tree. In *Proceedings of the 16th ACM SIGKDD International Conference on Knowledge Discovery and Data Mining*. 2010.
- [15] MENCL, R., A Graph-Based approach to surface reconstruction. In *Computer Graphics Forum*. 1995, roč. 14, č. 3, pp. 445–456.
- [16] NEŠETŘIL, J., MILKOVÁ, E. a NEŠETŘILOVÁ, H., Otakar Borůvka on minimum spanning tree problem. In *Discrete Mathematics*. 2001, roč. 233, č. 1–3, pp. 3–36.
- [17] SHAMOS, M. a HOEY, D., Closest-point problems. In 16th Annual Symposium on Foundations of Computer Science. 1975, pp. 151–162.

Mgr. Šárka Voráčová, PhD.

Katedra aplikované matematiky Fakulta dopravní ČVUT v Praze Na Florenci 25, 110 00 Praha, Česká republika e-mail: sarka.voracova@cvut.cz

Pedal curves – a playground for generalizations

Gunter Weiss

Dedicated to Prof. Dr. Friedrich Manhart on the occasion of his 70th birthday

Abstrakt

Primárne téma "úpätnicové krivky a plochy" patrí do klasickej diferenciálnej geometrie euklidovskej roviny alebo priestoru. Zostrojujeme priesečníky dotyčníc krivky c s kolmými priamkami istého zväzku. Pre tento základný koncept však existuje neuveriteľné množstvo rôznych modifikácií a zovšeobecnení a je široko používaný v základných kurzoch matematiky aplikácia rôznych oblastí geometrie a matematiky. Okrem didaktických prínosov tohto učebného materiálu možno stojí za zmienku poukázať aj na kľúčové stratégie výskumu v geometrii/ matematike, stratégiu zovšeobecňovania a zjednocovania. Tu sa projektívne geometrické hľadisko javí ako veľmi užitočné. Článok sa snaží poskytnúť prehľad o existujúcich zovšeobecneniach a tiež pridáva niektoré ďalšie.

Kľúčové slová: pedálna krivka – úpätnica, pedálne zobrazenie, korelácia, Minkowského normovaná rovina, afinná normála, relatívna normála, priamková kongurencia

Abstract

Primarily the topic "pedal curves and surfaces" belongs to classical differential geometry in the Euclidean plane or space. One intersects the tangents of a curve c with orthogonal lines of a pencil. Meanwhile, for this basic concept there exist incredible many modifications and generalizations, and is widely used in undergraduate mathematics courses as an application of different parts of geometry and mathematics. Besides the didactical benefits of such an exercise material it might be worth pointing kev strategies for geometric/ mathematical research, the generalization strategy and the unifying strategy. Here the projective geometric point of view seems very helpful. The paper tries to give an overview of existing generalizations and adds some additional ones.

Keywords: pedal curve, pedal mapping, correlation, circle geometry, Minkowski normed plane, affine normal, relative normal, line congruence

1 Introduction

The topic "pedal curves and surfaces" interacts with elementary differential geometry, kinematics, analytic geometry and linear algebra, with polarity and inversion, and with classical algebraic geometry. The simplicity of the construction makes it a perfect and stimulating trainings material in mathematics courses. One intersects the tangents of a curve c with orthogonal lines of a pencil Λ , Fig. 1. The common point O of Λ is called the "pole" of the pedal construction. For references see e.g. [10], [23]. In a more abstract sense one combines a differentiable object and an orthogonality structure to define "pedality". Thereby the orthogonality structure can be extrinsic, e.g. Euclidean, or intrinsic, e.g. defined by the affine normals of the curve c. The extrinsic orthogonality structure can also be non-symmetric, e.g. the Birkhoff-orthogonality in Minkowski normed planes (c.f. [20]), or simply a non-involutoric projectivity in the real affine plane. There exist already far-reaching generalizations concerning the dimension and structure of the place of action, which lead to an unmanageable number of

references to this widely ramified topic. This can be noticed, when googling the concept "pedal curves", see [23]. For example, a classical generalization of the concept "pedal curve" replaces the pole O and its pencil of lines by the tangent set of a curve c. When we intersect pairs of orthogonal tangents of c and o, we then call the resulting curve c' the "orthoptic curve" of the two curves c and o, c.f. e.g. [26]. Another approach could use o to define a relative-differential geometric concept of an orthogonality. Here, and using affine normals of a planar curve, we speak of an "intrinsically defined orthogonality concept". Finally, it is obvious that the different viewpoints of pedality can be treated in higher dimensions, too. For example, line geometric generalizations seem to be a rather new topic.

Far from presenting a complete overview, the following chapters will deal with widely well-known modifications of the pedal construction. Thereby a unified geometric approach comes to the fore.

2 The basic construction

One intersects the tangents of a curve c with orthogonal lines of a pencil Λ , Fig. 1. The common point O of Λ is called the "pole" of the pedal construction. For analytic treatment, this point O always can be used as the origin of a (Cartesian) coordinate frame, see e.g. [2], [7], [6, p.161]. It seems useful to enclose the Euclidean plane by an ideal line and use projective coordinates. Let $a(t), b(t), c(t), t \in I \subseteq \mathbb{R}$, be functions with no common zero in I, then the equation a(t)x + b(t)y + c(t) = 0 describes the tangents of a curve c, and -b(t)x + a(t) = 0 describes their normal through the origin O, which we choose as the pole for the pedal construction. Their intersections P'(t) are the result of the formal cross-product $(c(t), a(t), b(t))^T \times (0, -b(t), a(t))^T$, (in projective coordinates $((x_0: x_1: x_2))$ of the enclosed Euclidean plane)

$$(a(t)^{2} + b(t)^{2} : -a(t)c(t) : -b(t)c(t))^{T}.$$
 (1)

This shows that, if a(t), b(t), c(t) describe an algebraic line curve c^* of degree m, (the class of the corresponding point curve c), then P'(t) traces an algebraic point curve c' of degree 2m.

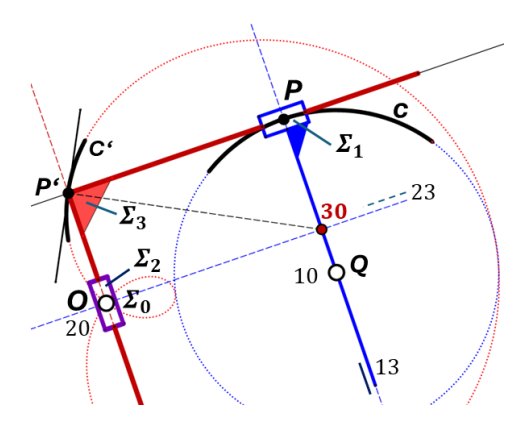


Fig. 1. The kinematic of the pedal motion with its map of instantaneous rotation centers allows to construct the tangent of the pedal curve c' of a curve c.

In Fig. 1 we add a kinematic generation of the curve c'. We take the fixed point O as belonging to the fixed plane Σ_0 and the moving system Σ_1 instantaneously rotating at $Q \in \Sigma_0$. This forces

the right-angle hook Σ_3 to slide through Σ_1 at P and through a system Σ_2 fixed at O and which rotates there. The instantaneous motion causes poles jk of Σ_j against Σ_k , such that we get the pole 30 of Σ_3 against Σ_0 via the so-called "three-pole theorem" of S. Aronhold-Kennedy, (see e.g. [12, p. 173], [24, p. 120], or [1]). This allows even to construct the tangent of c' at P'(t). The mapping of the tangent at $P(t) \in c$ to $P'(t) \in c'$ is called the "pedal mapping", and it can of course be applied to any point Y fixed in Σ_3 . Furthermore, the pedal mapping ψ maps line elements to line elements.

The very special construction of P' and the pedal mapping defined by c and O can also be seen as the product of a polarity at a circle ω with center O and the inversion at ω , see e.g. [4], [5] and Fig. 2. This allows to interpret the Euclidean construction also as performed in the Klein-model of a hyperbolic plane with ω as the "ideal conic", a Euclidean circle with pole O_1 as center, see Fig. 3.

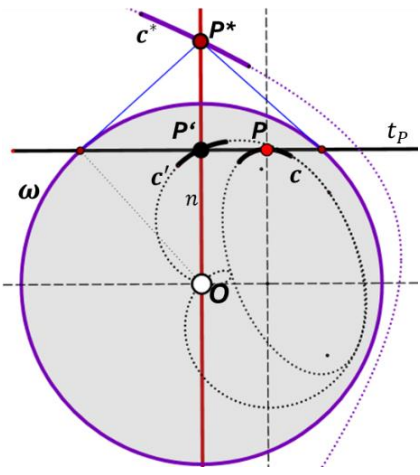


Fig. 2. Construction of the pedal point P' to a point P via the product of a polarity at a circle ω centered at the pole O and the inversion at ω .

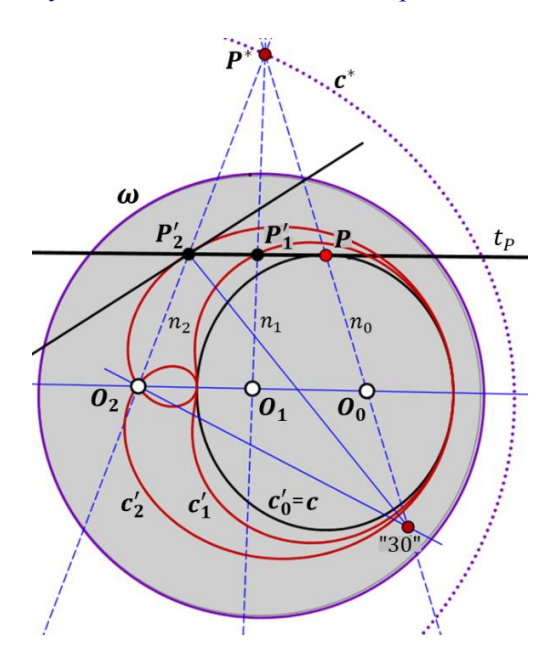


Fig. 3. Construction of the pedal points and curves of a circle c to different poles O_i in the F. Klein-model of a hyperbolic plane.

A simple generalization can replace the classical inversion by a Hirst inversion at an arbitrary conic, see [8], [9].

As the theorem of Aronhold-Kennedy is valid also the hyperbolic kinematic, it is possible to add also the hyperbolic modification of the construction of a tangent to the image curves c_i' , see the instantaneous pole "30" in Fig. 3 for the curve c_2' . Furthermore we can modify the classical inversion with a fixed circle ω and its center O to a "Hirst inversion" in a real projective plane π based on a real or imaginary conic ω and an arbitrarily chosen point O as center. By replacing the conic ω by its polarity $\overline{\omega}$ the well-known Hirst inversion is defined as a mapping ι : $\pi \to \pi$ with the property

$$\iota: X \mapsto X' \text{ with } X' = OX \cap X^{\overline{\omega}}$$
 (2)

As a first round-up we can formulate:

Result 1. The pedal point construction works in any Caley-Klein plane with non-degenerate orthogonality. The corresponding pedal mapping can be seen as the product of a polarity at a real or imaginary conic ω and a Hirst-inversion at ω with respect to a given pole O.

Remark 1. From the pedal point construction in the F. Klein-model of the hyperbolic plane it suggests itself to dualize the concept "pedal curve". We shall follow this extension of the concept "pedal curve" at another place.

3 Directly related concepts: negative- and contra-pedal curves legacy

References concerning pedal curves speak of the "negative pedal curve" as a modification of the classical pedal curve construction, see e.g. [10], [21], [23]. Let $\psi_0: c \to c'$ be the pedal mapping defined by c and pole O, then the reverse pedal mapping $\psi_0^{-1}: c' \to c$ is the negative pedal mapping defined by c' and the same pole O. This concept allows us to iterate the pedal point construction to both sides. For example, if c is a circle and we choose c0 then c0 then c1 is a point, and c2 simply the Thales circle over c1. Fig. 4 shows such an iteration with a circle c2 and the pole c3.

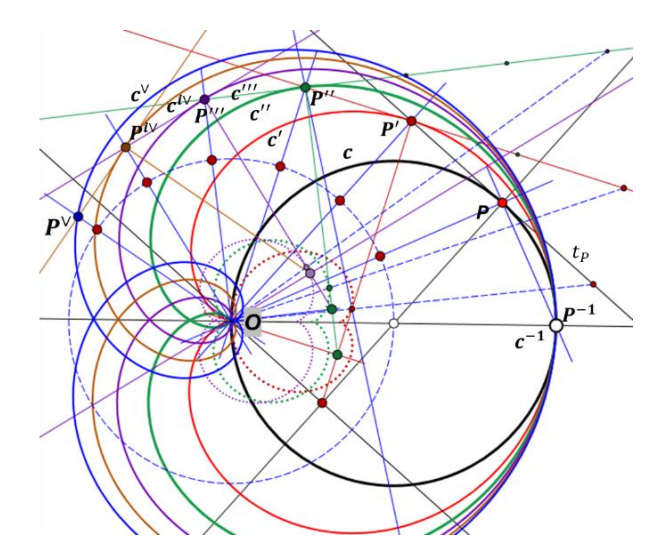


Fig. 4. Iteration of the pedal mapping starting with a circle c, in this case, together with the single negative pedal mapping.

It is obvious, that the orbit of points $P, Q \in c$ are logarithmic spiral polygons with spiral pole O, but they are not spirals of the same iterated similarity transformation. For example, the spiral polygons (P, P', P'', ...) and (Q, Q', Q'', ...) shown in Fig. 5 are not similar.

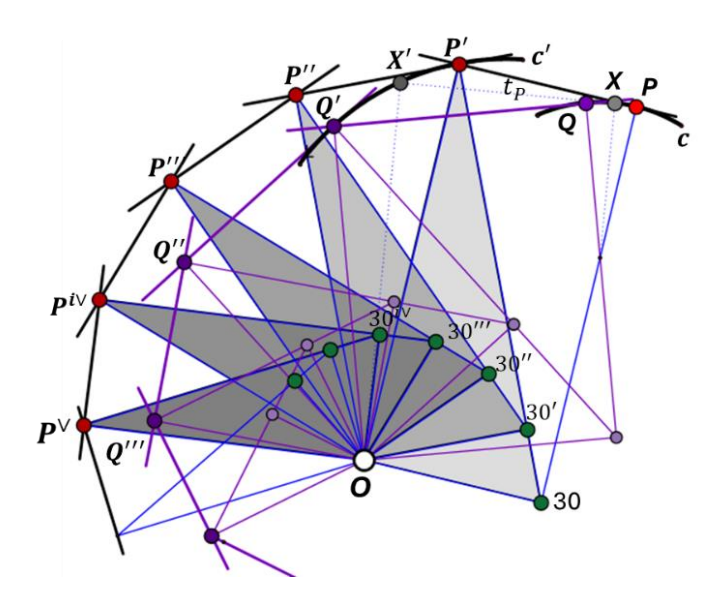


Fig. 5. The spiral polygons $\{P', P'', P''', \dots\}, \{Q', Q'', Q''', \dots\}$ to different points $P, Q \in c$ and derived by iterated pedal mappings belong to different spiral transformations.

The "contra-pedal curve" c' of a given planar curve c with respect to a pole O, see [10] and [23], is nothing but the pedal curve of the evolute c^* of c, see Fig. 6, where the pedal curves of an ellipse c and its evolute c^* is shown.

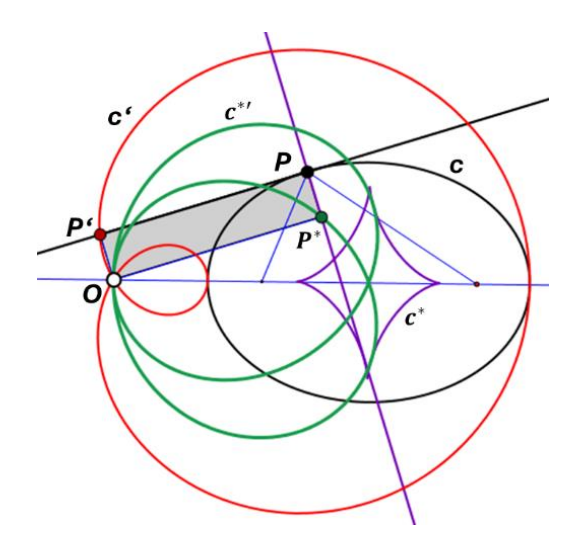


Fig. 6. The contra pedal curve of an ellipse c is the pedal curve $c^{*'}$ of its evolute c^* .

4 The pedal-mapping revisited

Let us, at first, look at the constructions shown in the previous chapters: The places of action are a real, projective enclosed affine plane or a projective plane with a Euclidean orthogonality concept. Furthermore, this Euclidean orthogonality concept can also be defined by the polarity of a circle. In the following we shall split these Euclidean approaches.

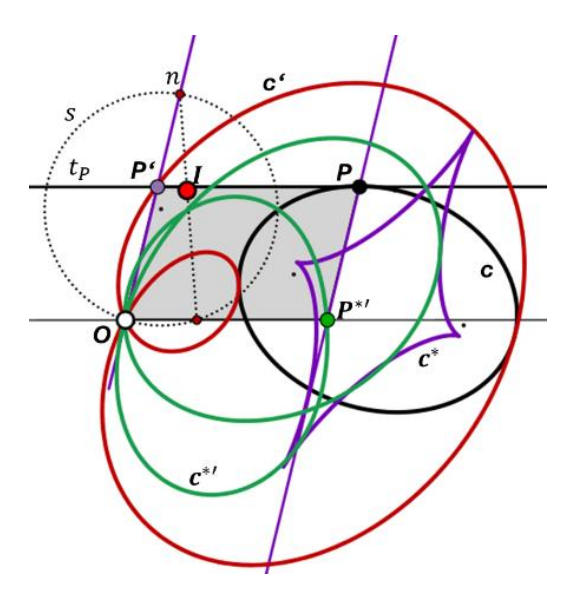


Fig. 7. The involutoric δ -orthogonality in the pencil Λ at O is completed via a Steiner-circle s and the involution center I. With this δ -orthogonality follows the construction of the pedal curve c' to a given curve c.

a) We start with a real affine plane, a curve c and a pole O. Let t_P be the tangent of c at a point $P \in c$ and $\bar{t}_P \parallel t_P$ the parallel line through O. In the pencil Λ of lines through O let an involutoric projectivity δ be given, e.g. the right-angle involution. Then \bar{t}_P^{δ} shall be defined as the δ -normal to t_P , and its intersection with t_P is the δ -pedal point P' to P. The graphic treatment will use a Steiner-circle s through O and an involution center I, (c.f. [3]), see Fig. 7. If I is an inner point of s, the involution δ is elliptic and the affine plane π together with the δ -orthogonality is Euclidean, while it is pseudo-Euclidean, if I is an exterior point of s.

(Note that δ induces, via the ideal points of the lines of the *O*-pencil, an absolute involution in the ideal line of π , see [3]).

For an analytic treatment we use O as origin and describe c by $\vec{x}(t) = (x(t), y(t))^T$, such that the direction vector of t_P is $\dot{\vec{x}}(t) = (\dot{x}(t), \dot{y}(t))^T$. An involution δ of the lines through O is described by a special regular 2 x 2 - matrix $M = (m_{ij})$, such that the direction vector of \bar{t}_P^{δ} is $M\dot{\vec{x}}(t)$.

As in Chapter 1 we use homogeneous coordinates in π and the convenient formal cross-product to calculate the coordinates of the pedal point P'(t) to P(t):

With

$$M = \begin{pmatrix} m_{11} & m_{12} \\ m_{21} & m_{22} \end{pmatrix} =: \begin{pmatrix} \overrightarrow{m}_1 \\ \overrightarrow{m}_2 \end{pmatrix}, t_P \triangleq \begin{pmatrix} \begin{vmatrix} x & y \\ \dot{x} & \dot{y} \end{vmatrix}, -\dot{y}, \dot{x} \end{pmatrix} \mathbb{R}, \ \overline{t}_P^{\delta} \triangleq \begin{pmatrix} 0, \overrightarrow{m}_1 \cdot \dot{x}, \ \overrightarrow{m}_2 \cdot \dot{x} \end{pmatrix} \mathbb{R}$$
(3)

the intersection $P' = t_P \cap \bar{t}_P^{\delta}$ is

$$P' \stackrel{\triangle}{=} \begin{pmatrix} -m_{11}\dot{x}^2 - (m_{12} + m_{21})\dot{x}\dot{y} - m_{22}\dot{y}^2 \\ -(x\dot{y} - y\dot{x})(m_{21}\dot{x} + m_{22}\dot{y}) \\ (x\dot{y} - y\dot{x})(m_{11}\dot{x} + m_{12}\dot{y}) \end{pmatrix} \mathbb{R} . \tag{4}$$

A regular matrix M describes, in general, a projectivity δ (different from an involution) in the ideal line of π , resp. in the line-pencil with vertex θ and it can be used to define a non-symmetric orthogonality in π . Therewith we can formulate:

Generalization 1. Given a regular curve c in an affine plane π , a pole O and a projectivity δ in the line-pencil at O to define a δ -orthogonality in π , then the pedal construction with this orthogonality delivers a δ -pedal curve c' to c.

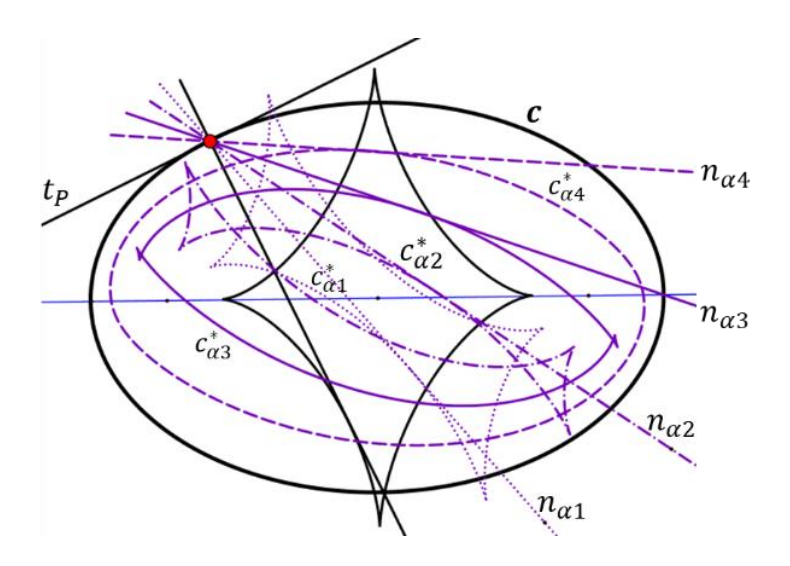


Fig. 8. Some pseudo-evolutes of an ellipse.

Remark 2. If M describes a Euclidean rotation δ , then the δ -normals enclose a fixed angle α with the tangents t_P of c. Especially the δ -normal at $P \in c$ envelops a so-called "pseudo-evolute" or "evolutoid" (c.f. [24, p. 241], [7], [8]), see Fig. 8. Obviously, the pedal construction delivers now an α -pedal curve as well as an α -contra-pedal curve, see Fig. 9a, b. Here it seems advisable to distinguish the "ortho-pedal points (curves)" from the "iso-pedal points (curves)".

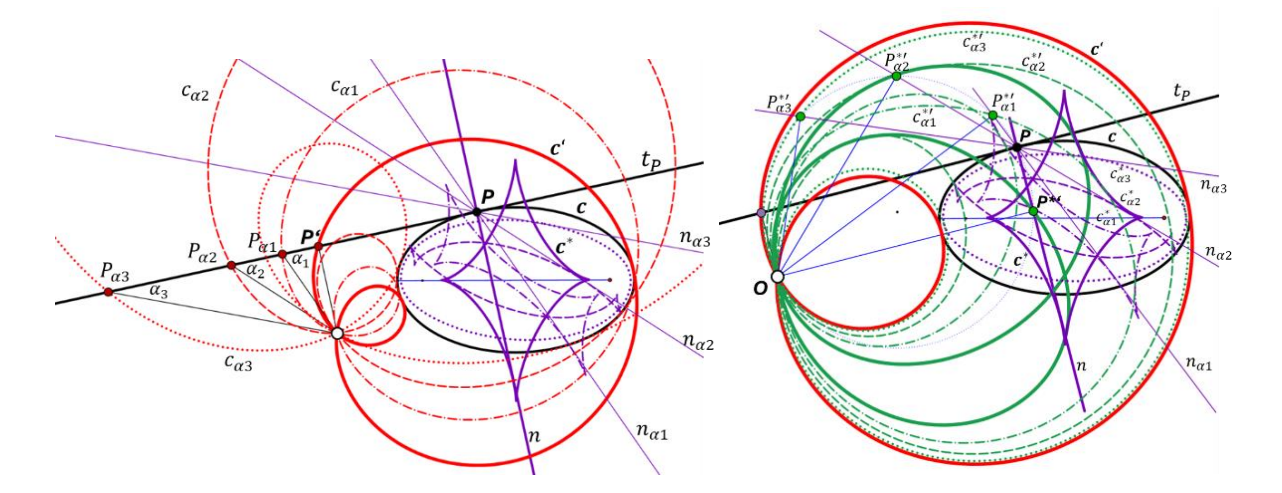


Fig. 9. a) Ortho-pedal curve c' and iso-pedal curves $c_{\alpha i}$ of an ellipse c, b) ortho-pedal curves $c_{\alpha i}^{*\prime}$ of the pseudo-evolutes $c_{\alpha i}^{*}$ of this ellipse c.

Let $P' \in t_P$ be the ortho-pedal point to $P \in c$ and Q' the ortho-pedal point to $Q \in t_\alpha^\delta$ of the pseudo-evolute c_α^δ , then $OP' \cap t_\alpha^\delta =: Q'_\alpha$ is the iso-pedal point of $Q \in c_\alpha^\delta$, and, vice versa, $OQ'_\alpha \cap t_P =: P'_\alpha$ is the iso-pedal point of $P \in c$. Obviously, the four points $P', P'_\alpha, Q', Q'_\alpha$ are concyclic, see Fig. 10.

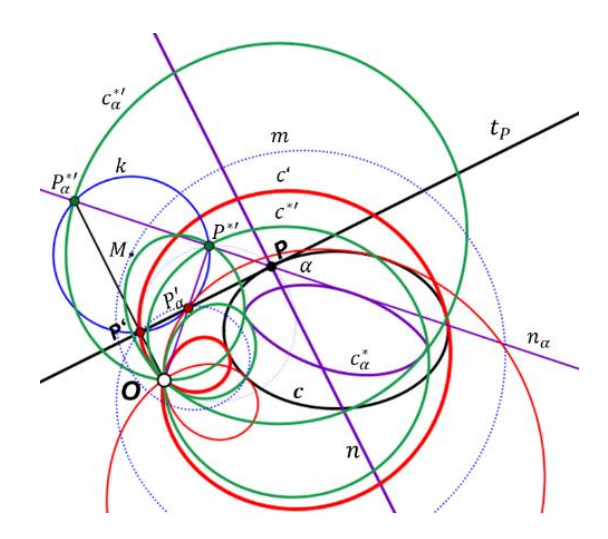


Fig. 10. Ortho- and iso-pedal points of a curve c and its pseudo-evolute $c_{\alpha i}^*$ form a concyclic quadrangle.

b) We generalize the polarity we used to get the point P^* to t_P , see Fig. 2, to a general correlation κ , but we replace the construction of P' via an inversion simply by intersecting t_P with the line OP^* . Obviously, the place of action now is the real projective plane π . This results in

Generalization 2. Given a regular curve c in a real projective plane π , a pole O and a regular correlation $\kappa: l \mapsto L^*$ of lines to points in π . Therewith it is possible to define a (in general not symmetric) κ -orthogonality of lines $l \in \pi$ to lines OP^* and use this to construct a κ -pedal curve c' to a given curve c.

5 The pedal-mapping in higher dimensions

- a) A well-known 3D-version of the pedal construction uses the Euclidean 3-space as place of action, a regular surface Φ , and a pole O. The pedal point P' to a regular point $P \in \Phi$ is defined as the intersection of the tangent plane τ_P at P with the normal $n \perp \tau_P$ through O. All properties of the basic 2D-situation, (e.g. the construction via polarity and inversion), can be directly transferred to this 3D-case. It is obvious that this pedal mapping and its properties can be transferred to any Euclidean n-space. But also the Generalizations 1 and 2 can easily be reformulated for real affine and projective n-spaces.
- **b**) Seemingly less considered is the case of a regular curve c in the Euclidean 3-space. We formulate the generalizations of pedal constructions related to c and a pole O as

Generalization 3. At a point $P(u) \in c$ we consider the Frenet-frame consisting of the tangent t_P , the main normal n_P and the binormal b_P . In addition, we shall consider the osculating plane $\sigma_P = t_P \vee n_P$, the normal plane $\nu_P = b_P \vee n_P$, and the rectifying plane $\rho_P = t_P \vee b_P$. Let now a pole O be given, then we can construct 6 Frenet-frame pedal points $T'_t(u)$, $N'_n(u)$, $B'_b(u)$, $S'_\sigma(u)$, $Q'_\nu(u)$, $R'_\varrho(u)$ to a point $P(u) \in c$, by intersecting the corresponding lines and planes of the Frenet frame with orthogonal elements through pole O.

Remark 3. In Generalization 3 we mentioned special lines and planes along c, but the essence is that c and its special line/plane sets can be replaced by any one-parametric set of lines or planes. Furthermore, we can start with an affine 3-space and define a δ -orthogonality by a regular correlation in the bundle of lines and planes through pole O, or, what means the same, an absolute δ -correlation in the ideal plane of the 3-space. This allows extending Generalization 3 to a 3D-version of Generalization 1. We leave the extension to higher dimensions to the reader.

Like for Generalization 2, we start with a real projective 3-space Π and a correlation κ in Π to define a κ -orthogonality structure for a pedal construction:

Generalization 4. Given a continuous one-parameter set of lines t or planes σ resp. a regular surface Φ , a pole O and a correlation κ in the real projective 3-space Π . Let P^* be the κ -image of the plane σ of c resp. of the tangent plane τ_P of Φ at a point P, then the κ -pedal point P' to σ , τ_P is the intersection of these planes with the line OP^* . For a line t and $t^* = \kappa(t)$, the κ -pedal point P' to t is the intersection of the plane $O \vee t^*$ with the line t.

6 A pedal-mapping in the line space of a 3-space

a) We extend the pole O of the former chapters to a line o, which we take as the polar line of a pedal construction. Let us, at first, start with a projective enclosed Euclidean 3-space and its Euclidean orthogonality \bot . (Concerning Euclidean line geometry consider e.g. [17], [22].) Based on the construction of the common perpendicular of two lines we formulate

Generalization 5. Given a set of lines $\{l_i\}$ in the projective enclosed Euclidean 3-space and a polar line o. The pedal point L_i of a line l_i is defined as the intersection point of l_i with the common perpendicular n_i of o and l_i .

We apply this proposal to the special elliptic line congruence \mathcal{L}^2 consisting of the left Clifford-parallels of a line z. We can consider this congruence as a set of reguli $\mathcal{R}_{1\Phi}(r)$ of coaxial and concentric hyperboloids of rotation $\Phi(r)$, and with common imaginary vertices at z, but also as a set of reguli $\mathcal{R}_{1\Psi}(\alpha)$ of orthogonal hyperbolic paraboloids $\Psi(\alpha)$ with common vertex Z and common vertex generator z. We use a Cartesian frame with origin Z and z as the third axis, and we consider a generator l = PQ with

 $P = r(\sin \alpha, \cos \alpha, 0)^T$, $Q = P + r(\sin \alpha, -\cos \alpha, 1/r)^T$, see Fig. 11.

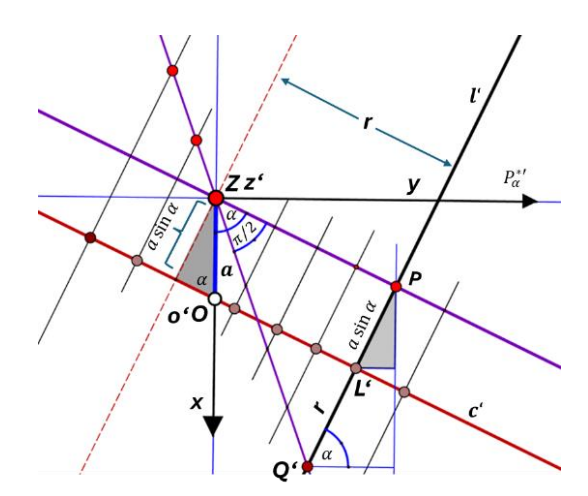


Fig. 11. Top-view image of $o \parallel z$ and of a generator $l(r, \alpha)$ of the special elliptic line congruence \mathcal{L}^2 and construction of the pedal point L of l.

The polar line $o \parallel z$ shall pass through $O = (a, 0, 0)^T$. For the top-view image L' of the pedal point L of l we find $\overline{PL'} = a \sin \alpha$, see Fig. 11. Therewith, L is the point

$$L(r,\alpha) = r \begin{pmatrix} \cos \alpha \\ \sin \alpha \\ 0 \end{pmatrix} + a \sin \alpha \begin{pmatrix} \sin \alpha \\ -\cos \alpha \\ 1/r \end{pmatrix}. \tag{5}$$

Keeping $\alpha = \alpha_0$ fixed, then (5) describes an equilateral hyperbola in a plane trough z parallel to $z \vee P(r, \alpha_0)$, see Fig. 12a. Keeping $r = r_0$ fixed, then (5) describes a rational curve $c = \{L(r_0, \alpha)\}$ on a hyperboloid of rotation $\Phi(r_0)$, see Fig. 12b. It is the pedal curve to the regulus $\mathcal{R}_{1,\Phi}(r_0)$. In rational homogeneous coordinates it is the curve

$$c = (r_0(1+t^2)^2, r_0^2(1-t^4) + 4ar_0t^2, 2r_0^2(t+t^3) - 2ar_0(t-t^3), 2ar_0(t+t^3)\mathbb{R}$$
 (6)

of degree 4 and Type II, i.e. a curve with the second regulus $\mathcal{R}_{2\Phi}(r_0)$ of $\Phi(r_0)$ as its tri-secants. Unexpectedly, the surface formed by the pedal points $L(r,\alpha)$ of all lines of the special elliptic line congruence is of degree 3. In cartesian coordinates it has the equation

$$z(x^2 + y^2) - a(xz + y) = 0. (7)$$

In Fig. 12b (top and front view projection) we show this pedal construction for a regulus $\mathcal{R}_{1\Phi}(r_0)$ of hyperboloid of rotation $\Phi(r_0)$ and with o parallel to its axis.

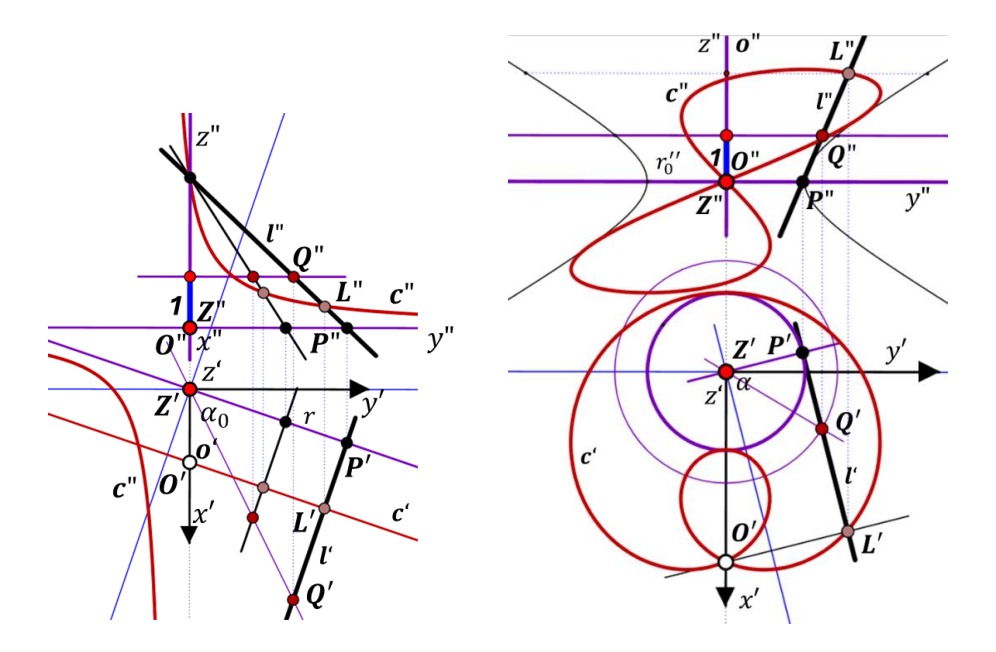


Fig. 12. a) Pedal point hyperbola c(α₀) for lines of the regulus R_{1Ψ}(α₀) of an orthogonal paraboloid of lines l∈ L²,
b) Pedal point curve c of degree 4 to the regulus R_{1Φ}(r₀) of lines l∈ L² of a hyperboloid of rotation.

Remark 4. Obviously, this procedure can be applied to any line set of dimension 1, 2 or even 3. In the latter case it results in a 3D-domain of pedal points. We omit here the discussion of exceptional lines and objects as well as of non-Euclidean geometries. We shall meet at least the pseudo-Euclidean orthogonality in Chapter 7.

Remark 5. It could also be of interest to translate the pedal procedure to F. Klein's point model of the line space which is a regular hyperquadric M_4^2 of index 2 in the real projective 5-space. Euclidean orthogonality of the original 3-space translates to the polar system of hypercone N_4^2 with its 2-dimensional vertex in M_4^2 . For references see e.g. [17], [22].

In higher dimensional Euclidean spaces we have the possibility to increase the dimension of the polar space. Here we cannot expect essentially new information about the resulting pedal point sets. Here we can therefore omit further discussions.

b) As another externally given orthogonality concept we might still use a regular correlation κ . We demand that it transforms the polar line o to a skew line $o^* = \kappa(o)$ and each plane ξ to a point $X^* = \kappa(\xi)$, and a line l, in general, to a skew line $l^* = \kappa(l)$. A modified pedal construction could be

Generalization 6. Given a polar line o and a regular correlation κ , then the pedal point X' of a plane ξ is the intersection of ξ with a line n_{ξ} through $X^* = \kappa(\xi)$ meeting o and $o^* = \kappa(o)$. Similarly, for a line l we get, in algebraic sense, a pair of pedal points, namely the intersections of l with the (in general two) lines $n_{l,1}, n_{l,2}$ meeting the (in general) four lines o, o^*, l, l^* .

To treat pedal constructions in the line-space, one could also use the polar system κ of a sphere Ω in the projective enclosed Euclidean 3-space. This allows to consider Ω , on one hand, as the absolute quadric of a hyperbolic space, similar as the 2-dimensional case and shown in Fig. 3, and on the other hand, an interpretation of Ω could be that of the Riemann sphere of the Möbius' circle geometry, what leads us to the next chapter.

7 Pedal-constructions in Euclidean circle geometries

We shall consider here Möbius' circle geometry and Laguerre's cycle geometry and connect the first one to the polar system ω of the Riemann sphere Ω in the Euclidean 3-space, while we interpret the second one as the cyclographic image of a 3-space, which is endowed with a pseudo-Euclidean metric, c.f. [16]. (Nevertheless, we have also the possibility to endow this pseudo-Euclidean space, in addition, with the Euclidean orthogonality.) While in the Möbius case a line l, via stereographic projection of Ω , maps to a pencil of circles through, in algebraic sense, two points, it is mapped via cyclographic projection to a linear set of cycles touching, in algebraic sense, two oriented lines, so-called spears. Roughly speaking, there is sort of a duality from one case to the other. (Concerning circle geometries consider e.g. [Ben].)

a) Pedal point construction in the Möbius plane

Given a pole O and a line l in the Euclidean 3-space, we aim at translating the construction of the pedal point L of a line l in space into a procedure for Möbius circles. Thereby we use the polar system ω to a sphere Ω , and the stereographic projection σ of Ω to the Möbius plane. A point X is mapped to a plane $\xi = X^{\omega}$, and σ maps the intersection $\Omega \cap \xi$ to a real, imaginary or degenerate Möbius circle X^M , according X is an exterior or interior point, or a point of Ω . A line l with only exterior points of Ω is mapped to a pencil of planes through the line $l^{\omega} \perp l$, which intersects Ω in two points F_1, F_2 , and all points $X \in l$ are finally mapped to real circles X^M of an elliptic pencil with fixed points F_1^M, F_2^M . All exterior points $Y \in l^{\omega}$ are mapped to real circles Y^M of a hyperbolic pencil with degenerate circles F_1^M, F_2^M . The inner points $Y \in l^{\omega}$ have imaginary circles (of this pencil) as Möbius images. The circles Y^M intersect all X^M orthogonally.

Now to the pedal construction: From the former chapter 6b) follows that the ω -normal $p \ni 0$ to l also intersects $l^{\omega} =: \bar{l}$. Therefore, p^{M} is a pencil of circles containing the solution circle $L^{M} \in l^{M}$ and a circle $\bar{L}^{M} \in \bar{l}^{M}$. Note that these three circles must have a common cord. We formulate at first an obvious

Corollary. The common cords of a fixed circle O^M and the circles X^M of a pencil form a pencil of lines. The common point Y of these cords is a point of the common y cord of all X^M .

The trivial proof applies the property of the power of a point with respect to a circle and can be read off from Fig. 13.

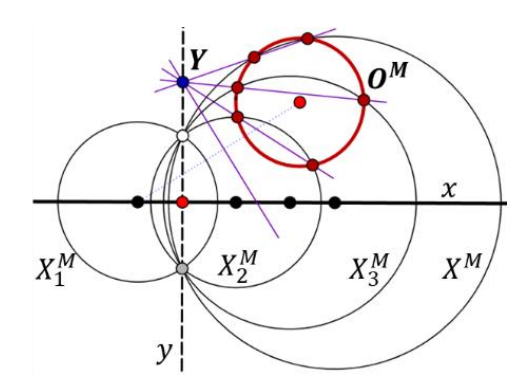


Fig. 13. The power of point $Y \in y$ with respect to circles O^M, X_i^M is constant

In application of this corollary we find a point Y on the common cord of l^M and a point X on the common cord of \bar{l}^M . The line XY is the common cord of o^M and the solution circles $L^M \in l^M$, $\bar{l}^M \in \bar{l}^M$. Thereby one of these solution circles can be imaginary, see Fig. 14a, b.

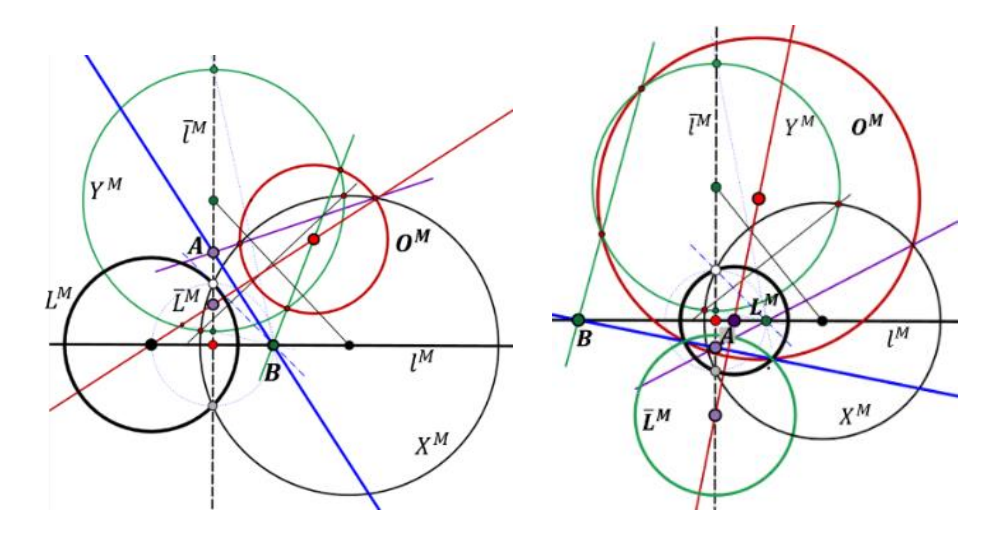


Fig. 14 a) and b). Construction in the Möbius plane of the Möbius images of the pedal points $L \in l, \overline{L} \in \overline{l}$ ($\overline{l} = l^{\omega}$) with respect to a point O. (left: L^M real, \overline{L}^M imaginary, right: L^M and \overline{L}^M real).

This basic construction can now be applied to sets of lines l, and, if we replace the pole O by a polar line o.

b) Pedal point construction in the Laguerre plane

The Laguerre plane consists of the set of cycles x^z , i.e. the set of oriented Euclidean circles and points of the Euclidean plane π , and of the set of spears t^z , i.e. the oriented lines of this plane. Each cycle x^z is described by the (cartesian) coordinate (x, y) of its center and its signed radius z and can be interpreted as the "cyclographic image" of a point X = (x, y, z) in space. One can say that x^z is the (oriented) trace of the right cone with vertex X and apex angle $\pi/2$, while a spear t^z stems of one of the planes through t^z with slope angle $\pi/4$. A spear t^z touches a cycle x^z , if the line of t^z touches the circle of t^z and the orientations at the touching point are the same. The (real or imaginary) tangential distance t^z 0 and calculates as

$$d_{ab} = \sqrt{(x_b - x_a)^2 + (y_b - y_a)^2 - (z_b - z_a)^2},$$
(8)

and this induces a *pseudo-Euclidean metric* in the so-called pe-space, see [16]. The orthogonality is ruled by the polarity ω of a real "absolute circle" c in the ideal plane of the pespace. Therefore, it is common use to speak of "c-geometry" with space-like, time-like and light-like slopes with respect to plane π . For references see e.g. [11] and [16]. A linear set of cycles is spanned by two cycles a^z , b^z and consists of all cycles x^z with the same (unique!) similarity center of x^z , b^z as that of a^z , b^z . They are therefore the cyclographic image of a line l in space.

According Result 1 the pedal point construction will work in this special Cayley-Klein space. In addition, we might endow the space with a Euclidean metric, too, and solve the problem of finding the pedal point L on a line l with respect to a pole $0 \notin \pi$ via the cyclographic mapping and the central projection with center 0, see Fig. 15.

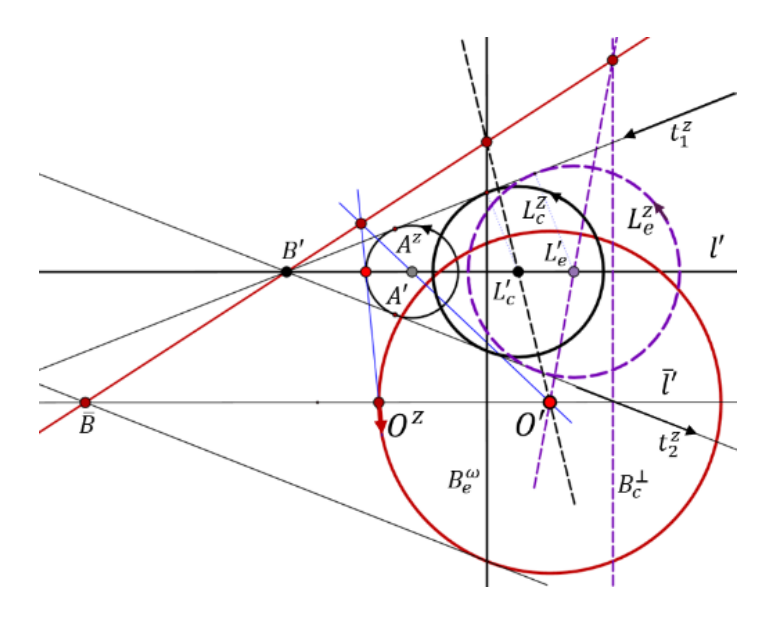


Fig. 15. The cyclographic images of the pedal point constructions in the *pe*-space and in the Euclidean space (dashed lines) via central projection with pole O as center.

Replacing O by a line $o \perp \pi$ according to the former chapter 6 we can construct the pedal cycles $L^z(\alpha)$ of a regulus $\mathcal{R}_{1\Phi}(r_0)$ of a "c-sphere" $\Phi(r_0)$, i.e. a hyperboloid of revolution intersecting the ideal plane in the absolute circle c. Note that, for $o \perp \pi$, Euclidean orthogonality is the same as pe-orthogonality. Fig. 16 shows the cyclographic image of the curve shown in Fig. 12b. The two arcs of the envelop of the resulting cycles belong to one algebraic curve, which is related to a nephroid.

We collect the procedures performed in this chapter as

Generalization 7. The classical pedal point constructions with respect to a pole O or a polar line o can be translated and modified to pedal circle constructions in the Euclidean Möbius and to pedal cycle constructions in the Euclidean Laguerre plane.

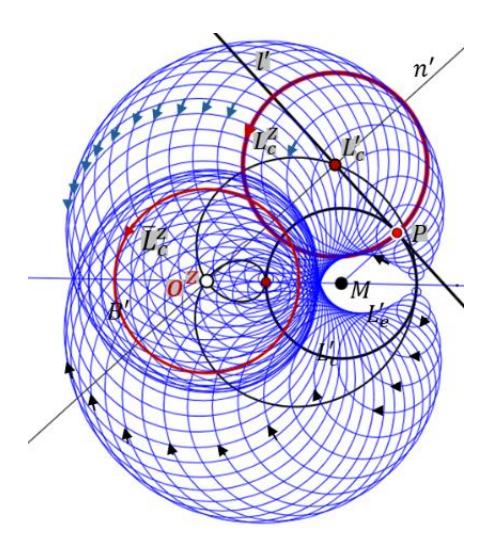


Fig. 16. Cyclographic image of the pedal curve c of Fig. 12b.

8 Pedal-constructions in affine planes with Minkowski-metric

A Minkowski plane is a real affine plane with a norm defined by a centrally symmetric, convex curve as "unit circle" c_M . In the following we demand that c_M is strictly convex and smooth. For Minkowski planes there exist many different orthogonality concepts. A purely of c_M induced is the nonsymmetric Birkhoff-orthogonality. Let P be a point of c_M , then the tangent t_P at P is *left-orthogonal* to the radius OP. For short, $OP \dashv t_P$, and $t_P \mid OP$ symbolizes right-orthogonal elements. For references see [20].

When one applies the pedal curve construction to c_M for the center O as pole, it is obvious that $c_M = c_M'$. Therefore, we can call c_M an "autopedal curve" with respect to pole O. Fig. 17a,b show the construction of the pedal curves c' to given curves c with respect to a pole O being the center of the Minkowski unit circle c_M . Based on the Birkhoff-left-orthogonality defined by c_M the Minkowski-evolutes c^* and, in Fig. 17b, also the pedal curve $c^{*'}$ of c^* are depicted.

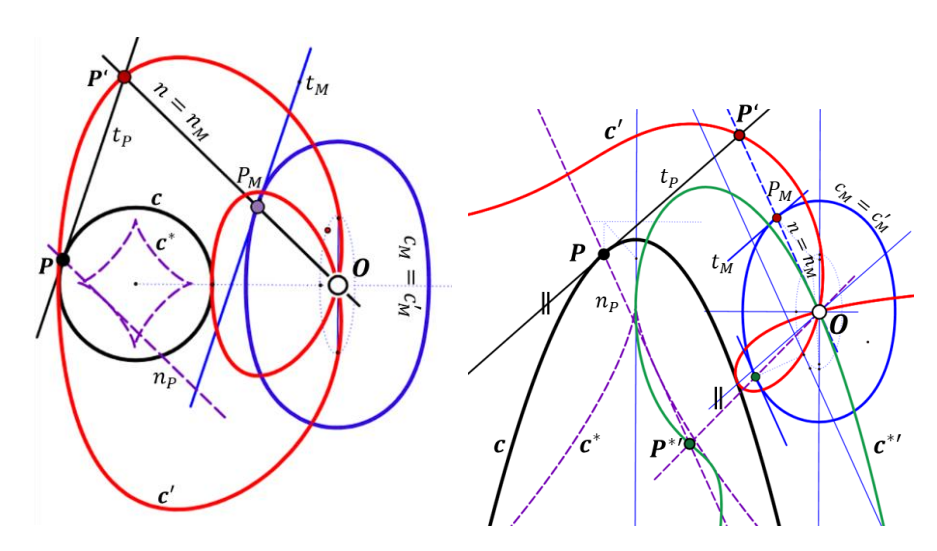


Fig. 17a, b. Minkowski pedal curve c' of a curve c based on Birkhoff-orthogonality with autopedal Minkowski unit-circle c_M .

One might also extend this construction principle to higher dimensions replacing the Euclidean unit-hypersphere by a strictly convex and smooth Minkowski unit-ball resp. unit-hyperball. For the planar case we formulate

Generalization 8. The classical pedal point constructions with respect to a pole O can directly be transferred to Minklowski-normed planes with a strictly convex and smooth Minkowski unit-circle c_M . Thereby, for a constructive treatment, e.g. Birkhoff left-orthogonality based on c_M replaces Euclidean orthogonality.

9 Pedal-constructions with intrinsically defined orthogonality

The construction principle presented in Chapter 8 seems closely related to an idea originally presented by Emil Müller in his "Lectures on Descriptive Geometry", namely the "relative differential geometry of curves and surfaces", see [15]. For further and actual references see e.g. [13]. In the following we shall consider two planar cases of orthogonality concepts, which are, more or less, intrinsically defined by the given curve c:

a) Relative geometric pedal curve construction

Let a C^2 -smooth curve c in the real affine plane π be given together with a vector field V_c along with c, as well as a pole O. When translating the vectors $\vec{n}_P \in V_c$ to point O, the tangent vectors \vec{t}_P of c induce a transversal parallel field along each line $n_{P,O}$ of the pencil $\{n_{P,O}\}$. Integrating this transversal field for a chosen starting point $Q \in n_{P_0,O}$ gives a curve c_R , which can be taken as a "relative unit-circle". With this relative unit-circle the construction of a pedal curve c' to c with respect to O and the given relative normal field can be performed like that for Minkowski planes. The only difference between the relative geometric case and the Minkowski geometric case is that c_R neither needs to be centrally symmetric nor O needs to be the center of an eventually symmetric curve c_R . Fig. 18 shows an example of a relative geometric pedal curve construction with c_R an arc of a parabola and the curve c_R as a Euclidean circle. Note that the relative orthogonality is not symmetric, see the construction of the contra-pedal point $P^{*'}$ of P in Fig. 18.

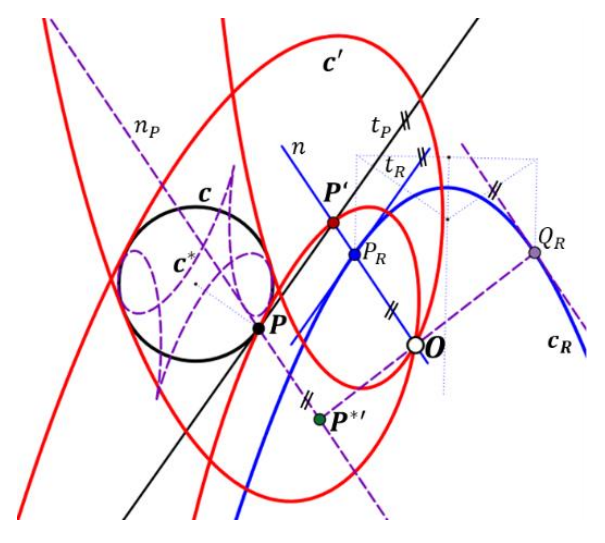


Fig. 18. Pedal point/curve and contra-pedal point construction with respect to a relative geometric orthogonality defined by the relative evolute c^* of c, leading to a relative unit arc c_R at pole O.

b) Pedal curve construction based on affine normals of a curve

A typical intrinsically defined orthogonality can be based on the affine normal field along a curve c in the affine plane π . With respect to affine transformations, the resulting pedal curve c' is even invariantly connected with the pair (c, 0). For references concerning Affine Differential Geometry see e.g. [18], [19]. We refrain here from a Figure, as the procedure is already described in the former part of this chapter.

Generalization 9. The construction of the pedal curve c' to a given pair (curve c, pole O) can be based on an orthogonality intrinsically connected with c, as e.g. a relative normal field or, especially, the affine normal field along c.

Obviously, it is possible to perform pedal point and pedal surface constructions also in the real affine space for a given triplet (surface Φ , relative normal field V_{Φ} , pole O). A given surface Φ allows a special set of intrinsically defined relative normal vector fields V_{Φ} , see e.g. [13].

10 Replacing the pole O by a curve o: orthoptics and isoptics.

We restrict the considerations to the Euclidean plane π and replace the pole O by a regular curve o. Given a regular curve c, its pedal curve c' is the set of intersection points P' of tangent t_P at a point $P \in c$ with all tangents $t_O \perp t_P$ of o. This means that c' is the "orthoptic" of the pair (c,o). When we, according to Generalization 2, replace the right angle by a constant $\alpha = \angle t_P t_o$, we receive a curve c'_α , which now acts as "isoptic" of the pair (c,o). We mention this as

Generalization 10. Orthoptics of pairs of two curves c and o can be seen as ortho-pedal curves of the pair (c, o), while isoptics of such a pair of curves are their α -pedal curve.

For orthoptics and isoptics there are many references, see e.g. see e.g. [14], [23], [26]. Fig. 19a, b and Fig.20a, b show both types of such curves for rather simple pairs (*c*, *o*).

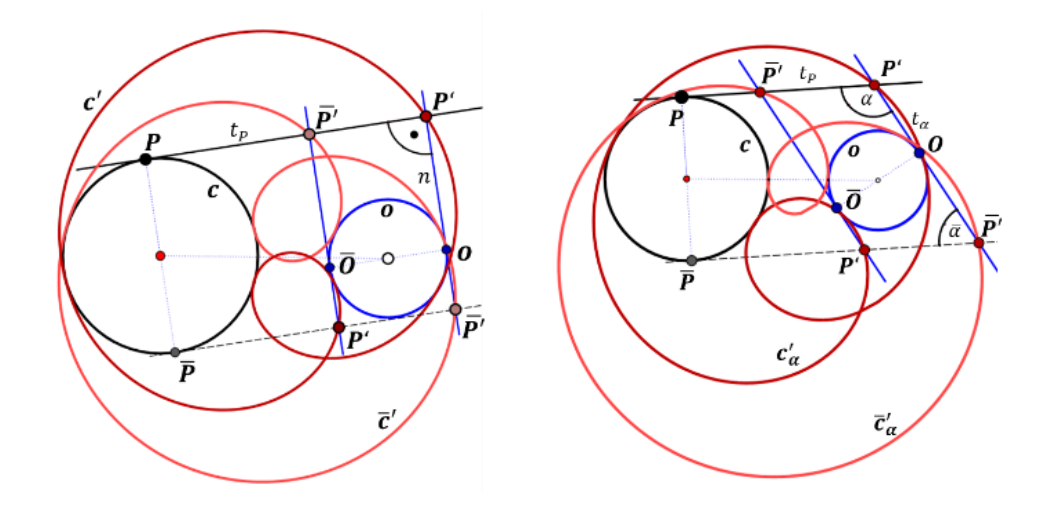


Fig. 19a, b. The orthoptics c', \bar{c}' and isoptics c'_{α} , \bar{c}'_{α} of a pair of circles (c, o).

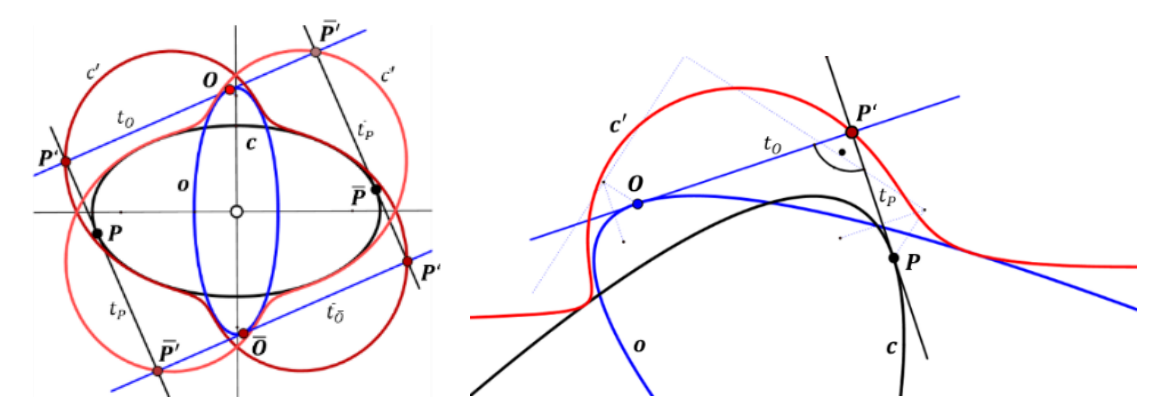


Fig. 20a, b. The orthoptics c', \bar{c}' of a pair of ellipses and of parabolas (c, o).

How to adapt these planar constructions for orthogonal elements in space? Instead of a curve c we can take a surface Φ and instead of the tangents t_P the set of tangent planes τ_P in the points $P \in \Phi$. In the plane we replaced the pencil of lines $n \ni 0$ by the (one-dimensional) set \mathcal{L}^1 of tangents of a curve o. Therefore, we should use a two-dimensional set of lines \mathcal{L}^2 in space and look for the lines $n \in \mathcal{L}^2$ orthogonal to each of the planes τ_P . The pedal point P' of τ_P is then its intersection with n. The set \mathcal{L}^2 is called "line congruence". It can be defined as the set of common tangents of two surfaces or the set of lines intersecting two curves or mixed. Especially linear line congruences meet, in algebraic sense, two lines, and we considered already the very special congruence \mathcal{L}^2 with rotational symmetry in chapter 6. Extending Generalization 10 to higher dimensions we can formulate

Generalization 11. A way to adapt the planar orthoptic for a construction in space is to intersect the tangent planes of a surface Φ with orthogonal lines out of a line congruence \mathcal{L}^2 . For adapting it to an n-space, the tangent hyperplanes of a hyper-surface had to be intersected with orthogonal lines of an (n-1)-dimensional set \mathcal{L}^{n-1} of lines.

We finish this chapter with the construction of the pedal points P_{τ} of the tangent planes τ_P of a sphere Φ with respect to the special linear line congruence \mathcal{L}^2 having rotational symmetry (as used in the Fig. 11, 12a, b), see Fig. 21.

For a fixed angle α_0 , i.e. a chosen meridian $m(\alpha_0) \in \Phi$, we must intersect a cylinder of revolution $\Gamma(\alpha_0)$ with an orthogonal hyperbolic paraboloid $\Psi(\alpha_0)$, whereof one vertex generator coincides with the axis of $\Gamma(\alpha_0)$.

The short calculation for a sphere Φ with radius r and centered in the origin Z, and the special line congruence \mathcal{L}^2 with z as rotation axis and centered in Z, delivers the equation of the pedal surface Φ'_{r^2} as

$$\Phi'_{\mathcal{L}^2} \dots z^2(x^2 + y^2 + z^2 - r^2 + 1) - r^2 = 0$$
 (9)

The top view c' of the pedal curve $c = \Gamma(\alpha_0) \cap \Psi(\alpha_0)$, see Fig. 21, and for $\alpha_0 = \pi/2$ is described by

$$x^2(y^2+1) = r^2y^2 . (10)$$

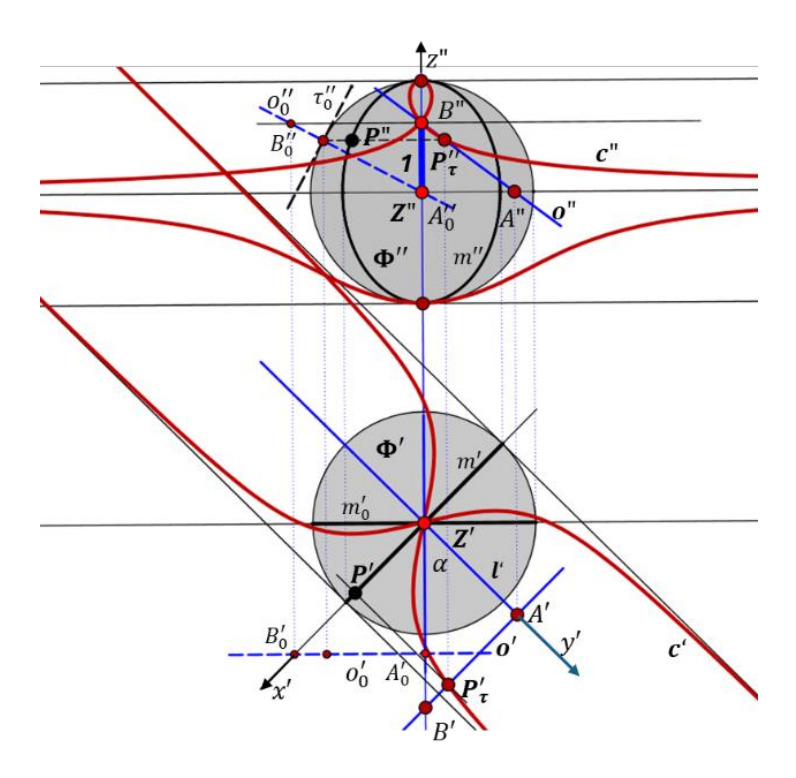


Fig. 21. Pedal curve c for tangent planes τ_P along a meridian m of a sphere Φ with respect to a special elliptic linear line congruence \mathcal{L}^2 .

11 Final remark and conclusion

The presented material of generalizations of the classical pedal curve construction shall shows strategies and possibilities, how to generalize a mathematical topic: increasing the dimension and/or changing of the key structure of the place of action. Most of the 11 generalizations mentioned above can be used as exercise material for research topics for their own, like e.g. non-Euclidean kinematics, circle geometries, line geometry, and relative and affine differential geometry. As it would extend the paper furthermore, we skipped here the dualization of the pedal point/curve construction, which, in some sense, connects the standard pedal construction to the topic of tractrices, see e.g. [28].

Here the treatment is kept at low level, such that it could be used also in undergraduate geometry and mathematics courses. Concerning the figures, which are made uniquely with the free graphics software Cinderella, one can at least see that simple descriptive geometry still is quite an effective research tool worthy to be kept alive.

References

- [1] "Aronhold-Kennedy Theorem": https://scienceeureka.com/aronhold-kennedy-theorem/#:~:text=The%20Aronhold%20Kennedy%20Theorem
- [2] BOHNE, E., KLIX, W-D., *Geometrie Grundlagen für Anwendungen*, p. 345, Fachbuchverlag Leipzig-Köln 1995, ISBN 3-343-00887-7.

- [3] BRAUNER, H., *Geometrie projektiver Räume*, (Geometry of projective spaces), B.I. Wissenschaftsverlag, Zürich 1976, ISBN 3-411-01513-6.
- [4] DIRNBÖCK, H., Kinematic properties of the Negative Pedal Motion with one Path as an Ellipse. (privately published as Op. 246 (2021), authors address: Am Rautkogel 15, A-9061 Klagenfurt Wölfnitz, Austria).
- [5] DIRNBÖCK, H., Die Fußpunkts-Transformation Wiederholungen. (privately published as Op. 303 (2023), authors address: Am Rautkogel 15, A-9061 Klagenfurt Wölfnitz, Austria).
- [6] EDWARDS, J., Differential Calculus. London: MacMillan and Co. (1892).
- [7] GLÄSER, G., Geometry and its Applications in Art, In *Nature and Technology*. Springer Wien New York 2012, pp. 338 368, ISBN 978-3-7091-1450-6.
- [8] GLÄSER, G., STACHEL, H., ODEHNAL, B.: The Universe of Conics, 2nd ed., Springer Spektrum, Heidelberg 2024, ISBN 978-3-662-70305-2.
- [9] "Hirst inverse", see .maths.gla.ac.uk/wws/cabripages/triangle/ninepoint/hirstinverse.htm
- [10] KÖLLER, J., Mathematische-Basteleien.de/Fußpunktkurve.htm, (Januar 2016).
- [11] KRAMES, J.L., *Die Zyklographie* (the cyclographic projection), Vol. II of E. Müller's "Vorlesungen über Darstellende Geometrie". Franz Deuticke, Leipzig und Wien 1929.
- [12] KRUPPA, E., *Analytische und konstruktive Differentialgeometrie*, (Analytic and constructive differential geometry), Springer-Verlag, Wien 1957.
- [13] MANHART, F., Relativgeometrische Kennzeichnungen euklidischer Hyperprivatsphären. In *Geometriae Dedicata* 29(2)/1989, pp. 193-207. DOI: 10.1007/BF00182120
- [14] Mathcurve: https://mathcurve.com/courbes2d/isoptic/isoptic.shtml 15
- [15] MÜLLER, E., Punktmittenflächen und eine Art relativer Flächentheorie. (Point-midpoint-surfaces and sort of a theory on relative differential geometry of surfaces.) Sitzungsberichte d. Akad. d. Wiss. in Wien. Math.-naturw. Kl., Abt. II a, Bd. 134 (1925).
- [16] https://en.wikipedia.org/wiki/Pseudo-Euclidean space Wikipedia
- [17] POTTMANN, H., WALLNER, J., Computational Line Geometry, Springer-Verlag, Berlin-Heidelberg 2001, p. 176, ISBN 3-540-42058-4
- [18] SALKOWSKI, E., *Affine Differential Geometrie*. (Göschens Lehrbücherei: Pure and Applied Mathematics Vol. 22). De Gruyter, Berlin 1934, Reprint 2019, ISBN 978-3-11-098975-5.
- [19] SCHIROKOW, P. A., SCHIROKOW, A. P., Affine Differentialgeometrie. Teubner, Leipzig 1962.
- [20] THOMPSON, A.C., *Minkowski Geometry*. Cambridge University Press 1996, ISBN: 9781107325845 (online publ. May 2013).
 DOI: https://doi.org/10.1017/ CBO9781107325845
- [21] UEDA, K., Pedal curves and surfaces, (p. 497 506 in Mathematical Methods for Curves and Surfaces: Oslo 2000, ed. Lyche, T., Schumaker, L.L), Vanderbilt University, Computer Science Dept., Nashville, TN, USA 2001, ISBN:978-0-8265-1378-6.
- [22] WEISS, G., Zur euklidischen Differentialgeometrie der Regelflächen, (To the Euclidean Differential Geometry of Ruled Surfaces). Resultate d. Math. Vol 6 (1983), pp. 220-250.

- [23] WEISSTEIN, E.W., CRC Encyclopedia of Mathematics. ark: /13960/t1kh1wc8f. "Math World", htttps://en.wikipedia.org/wiki/MathWorld
- [24] WUNDERLICH, W., *Ebene Kinematik* (Hochschultaschenbuch 447/447a). Bibliograph. Inst. Mannheim, 1970.
- [25] WUNDERLICH, W., Kurven mit isoptischem Kreis. In Aequat. math. 6 (1971), pp. 71-81.
- [26] WUNDERLICH, W., Die isoptischen Kurven der Zykloiden. In Zeitschrift f. Angew. Math. u. Mech. 17 (1937), 56.
- [27] WUNDERLICH, W., Über die Schleppkurven des Kreises. Sitzungsber., Abt.II, Österr. Akad. Wiss., Math.-Naturw. Kl. 156 (1948), pp. 155–173.
- [28] WUNDERLICH, W., Über die Hundekurven mit konstantem Schielwinkel. In Monatsh. Math. 61 (1957), pp. 277–311.

Gunter Weiss, ret. professor

University of Technology Vienna, Austria University of Technology Dresden, Germany email: weissgunter@gmx.at

Abstracts

P. Salvi: The curves of Eduard Lehr

The class of curves whose curvature is a trigonometric function of the arc length has appeared multiple times in the last century, in different contexts. It was first studied by Eduard Lehr, in a relatively obscure work. Due to renewed interest in it within the field of aesthetic curves [8], we summarize its most important results in this paper.

Š. Voráčová: MST-based clustering for curve and surface reconstruction

The Minimum Spanning Tree problem has been referenced in the literature as early as 1926, making it one of the oldest and most thoroughly studied problems in computational geometry. Alongside its enduring theoretical and algorithmic appeal, the MST is valuable for addressing numerous practical data analysis problems as well as image segmentation and reconstruction of the curve and surfaces.

In this paper, we present curve and surface reconstruction methods using the Euclidean MST algorithm. The MST can help ensure that the reconstructed curve is efficient in terms of connectivity and distance.

G. Weiss: Pedal curves – a playground for generalizations

Primarily the topic "pedal curves and surfaces" belongs to classical differential geometry in the Euclidean plane or space. One intersects the tangents of a curve c with orthogonal lines of a pencil. Meanwhile, for this basic concept there exist incredible many modifications and generalizations, and it is widely used in undergraduate mathematics courses as an application of different parts of geometry and mathematics. Besides the didactical benefits of such an exercise material it might be worth pointing to a key strategies for geometric/ mathematical research, the generalization strategy and the unifying strategy. Here the projective geometric point of view seems very helpful. The paper tries to give an overview of existing generalizations and adds some additional ones.

G

Slovak Journal for Geometry and Graphics

Volume 22 (2025), No. 43 ISSN 1336-524X

Edited by:

Slovak Society for Geometry and Graphics

SSGG

Editor-in-Chief: Daniela Velichová

Managing Editors:

Dagmar Szarková Daniela Richtáriková

Editorial Board:

Ján Čižmár Andrej Ferko Pavel Chalmovianský Mária Kmeťová Margita Vajsáblová G is a scientific journal covering the fields of geometry and graphics for publication of original scientific papers, review and information articles, reports, state-of-the-art reviews, communications and other contributions from all geometric disciplines (elementary, descriptive, constructive, projective, coordinate, differential, algebraic, computer, computational, finite, non-Euclidean) and topology, geometric modelling and computer graphics, in the area of the basic theoretical research, education of geometry in all types of schools, from the history and methodology of the development of geometry and on applications of geometry and geometric methods in different scientific, social or technical disciplines.

Editorial office: Slovak Society for Geometry and Graphics

IČO: 31 816 304

Faculty of Mechanical Engineering

Slovak University of Technology in Bratislava

Námestie slobody 17 812 31 Bratislava, Slovakia

Correspondence concerning subscriptions, claims and distribution:

Redakcia G - SSGG

SjF STU, Námestie slobody 17, 812 31 Bratislava, Slovakia

ssqq@ssqq.sk

Frequency: One volume per year consisting of two issues at a price of EUR 20,- per

volume, not including surface mail shipment abroad.

Evidentiary number EV 3228/09

Information and instructions for authors are available at the address: www.ssgg.sk

Printed by: ForPress Nitrianske tlačiarne, s.r.o.

G is indexed in: Zentralblatt für Mathematik

Copyright © SSGG September 2025, Bratislava, No. 1/2025

All rights reserved. No part may be reproduced, stored in a retrieval system, or transmitted in any form or by any means, electronic, mechanical, photocopying, recording, or otherwise, without prior written permission from the Editorial Board. All contributions published in the journal were reviewed with respect to their scientific

www.ssgg.sk